AD-A092 707 OHIO STATE UNIV COLUMBUS DEPT OF GEODETIC SCIENCE F/G 8/5
GEOID HEIGHTS, GEOID HEIGHT DIFFERENCES, AND MEAN GRAVITY ANOMA--ETC(U)
JUN 80 R RUMMEL F19628-79-C-0027
UNCLASSIFIED DGS-306 AFGL-TR-80-0294 NL

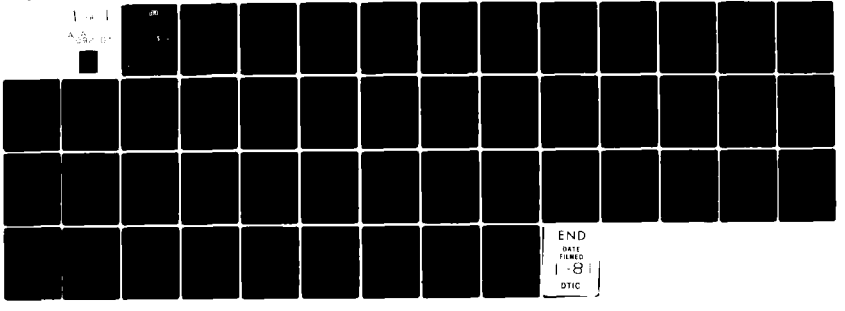

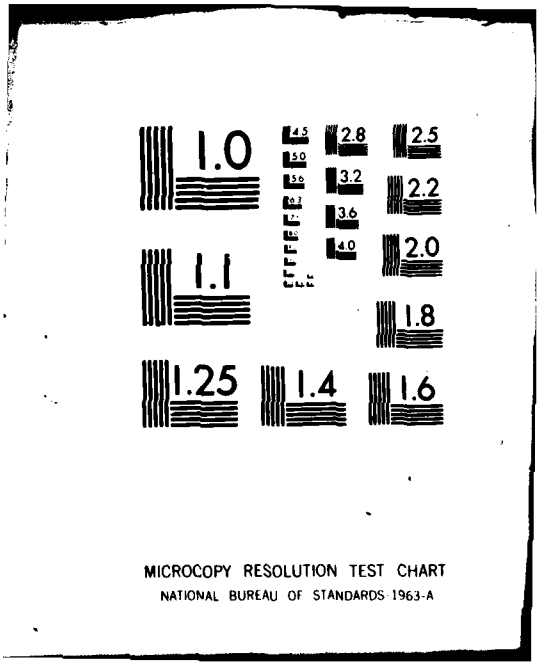
1.0
1.1
1.25
1.4
1.6
1.8
2.0
2.2
2.5
2.8
3.2
3.6
4.0
4.5
5.0
5.6
6.3
7.1
8.0
9.0
MICROCOPY RESOLUTION TEST CHART
NATIONAL BUREAU OF STANDARDS 1963-A

AFGL-TR-80-0294

GEOID HEIGHTS, GEOID HEIGHT DIFFERENCES, AND MEAN GRAVITY ANOMALIES FROM "LOW-LOW" SATELLITE-TO-SATELLITE TRACKING - AN ERROR ANALYSIS

Reiner Rummel

The Ohio State University
Research Foundation
Columbus, Ohio 43212

June, 1980

Scientific Report No. 6

AIR FORCE GEOPHYSICS LABORATORY
AIR FORCE SYSTEMS COMMAND
UNITED STATES AIR FORCE
HANSCOM AFB, MASSACHUSETTS 01731

Unclassified

SECURITY CLASSIFICATION OF THIS PAGE (When Data Entered)

REPORT DOCUMENTATION PAGE	READ INSTRUCTIONS BEFORE COMPLETING FORM
1. REPORT NUMBER: AFGL-TR-80-0294	2. GOVT ACCESSION NO.: AD-A092 707
3. RECIPIENT'S CATALOG NUMBER: DGS-306, SCIENTIFIC-6	
4. TITLE (and Subtitle): GEOID HEIGHTS, GEOID HEIGHT DIFFERENCES, AND MEAN GRAVITY ANOMALIES FROM "LOW-LOW" SATELLITE-TO-SATELLITE TRACKING - AN ERROR ANALYSIS	5. TYPE OF REPORT & PERIOD COVERED: Scientific Report No. 6
	6. PERFORMING ORG. REPORT NUMBER: Dept. of Geod. Sci. No. 306
7. AUTHOR(s): Reiner Rummel	8. CONTRACT OR GRANT NUMBER(s): F19628-79-C-0027
9. PERFORMING ORGANIZATION NAME AND ADDRESS: Department of Geodetic Science, The Ohio State University - 1958 Neil Avenue, Columbus, Ohio 43210	10. PROGRAM ELEMENT, PROJECT, TASK AREA & WORK UNIT NUMBERS: 61102F, 2309G1AW
11. CONTROLLING OFFICE NAME AND ADDRESS: Air Force Geophysics Laboratory, Hanscom AFB, Massachusetts 01730, Contract Monitor: Bela Szabo/LW	12. REPORT DATE: June 80
	13. NUMBER OF PAGES: 44
14. MONITORING AGENCY NAME & ADDRESS (If different from Controlling Office)	15. SECURITY CLASS. (of this report): Unclassified
	15a. DECLASSIFICATION/DOWNGRADING SCHEDULE

16. DISTRIBUTION STATEMENT (of this Report)

A - Approved for public release; distribution unlimited

17. DISTRIBUTION STATEMENT (of the abstract entered in Block 20, if different from Report)

18. SUPPLEMENTARY NOTES

19. KEY WORDS (Continue on reverse side if necessary and identify by block number)

satellite-to-satellite tracking, error analysis, gravity anomalies, geoid heights

20. ABSTRACT (Continue on reverse side if necessary and identify by block number)

The mathematical model for a simultaneous estimation of improved orbital parameters and an approximation of the earth's gravity field from range rate observations in an SST "low-low" experiment is described. In a somewhat simplified model an error analysis for the estimation of geoid heights, geoid height differences 1° x 1° mean gravity anomalies is performed employing the least squares collocation method. Investigated is the dependence of the estimated parameters upon the

DD FORM 1 JAN 73 1473 EDITION OF 1 NOV 65 IS OBSOLETE

Unclassified

SECURITY CLASSIFICATION OF THIS PAGE (When Data Entered)

measurement precision, the spatial configuration of the two satellites, the inter-satellite distance, and the experiment altitude. In an optimal situation - assuming a range rate precision of $\pm 10^{-5}$ ms^{-1}, an intersatellite distance of 250 km, and an experiment altitude of 200 km - the estimated a posteriori std. dev. are $\pm$ 0.9 m for point geoid heights, $\pm$ 0.7 m for geoid height differences (point seperation 150 km), and $\pm$ 6 to 7 mgal for $1^{\circ} \times 1^{\circ}$ mean gravity anomalies. These numbers compare very well with the results obtained from GEOS-3 altimetry for the seasurface topography. Unmodelled short-wavelength uncertainties in the orbit have thereby to be controlled down to 1 cm in radial direction, whereas the requirements for the control of long-wavelength error effects are moderate.

Table of Contents

1. Introduction

As a result of the December 1978 workshop session of the panel on gravity field and sea level requirements the resulting report "Applications of a Dedicated Gravitational Satellite Mission" (1979) contains a discussion on the kind and precision of gravity parameters to be provided through a dedicated gravitational satellite mission. These requirements are in essence:

1. For geological or geophysical applications gravity data (gravity anomalies ?) with a half-wavelength resolution of down to 100 km and an accuracy of ± 2.5 to 10 mgals depending on the application;
2. Oceanographers would need geoid height differences for distances of 100 to 3000 km with an accuracy of ± 10 cm.

The same report contains, in addition, a list of open questions concerning e.g. the assumptions on the range rate data noise, the needed orbital accuracies, the "best" gravity parameterization, the appropriate error measure a.s.o., to be analyzed in further studies.

The purpose of this report is to answer part of these questions in an error analysis for *satellite-to-satellite tracking* (SST) in the low-low mode. For the influence of systematic and random uncertainties of the satellite orbit upon the gravity estimates, a problem of high relevance, which is considered in Douglas et al. (1980) too, sensitivity coefficients are derived. The study will also analyze the dependency of the accuracy of the estimated gravity parameters on the measurement precision, the altitude of the satellite, the separation and spatial arrangement, and on the data coverage. As a conclusion of the above stated user requirements the estimated parameters will be on one hand $1^\circ \times 1^\circ$ mean gravity anomalies (for geophysical purposes) and on the other hand geoid heights, and geoid height differences, respectively, (for oceanographers). The estimation model that allows without difficulties this type of flexibility is the least squares collocation model. Because of some conceptual problems, this model will be simplified, without any serious impact on the validity of the results, however. Special attention will be put on the definition of a valid concept for the error measure.

This study may be considered as complementary to those of Schwarz (1970) and Kaula et al (1978) in that a different type of mathematical model is employed, to Krynski (1978) because of the more operational type of model, and to Rummel (1979) where for a purely theoretical model the optimal situation is analyzed. It is also complementary to Rapp and Hajela (1979) who discuss in a very similar manner the corresponding SST high-low case.

2. Observational Model for Range Rates

The range rate $\dot{\rho}$ between two satellites at S_1 and S_2 is expressed as

$$\dot{\rho}(S_1, S_2) = \dot{\underline{X}}_{12} \cdot \underline{e}_{12}, \tag{1}$$

where $\dot{\underline{X}}_{12} = \dot{\underline{X}}(S_2) - \dot{\underline{X}}(S_1)$ is the velocity difference between the two space probes, and $\underline{e}_{12} = \rho^{-1} \underline{X}_{12}$, the unit vector pointing from S_1 (with position vector $\underline{X}_1$, expressed e.g. in an quasi-inertial frame) to S_2 and ρ is their distance. From equation (1) the observational model will be derived, similar to the model in Rummel et al. (1978) and according to guidelines developed in Grafarend (1979). [Neither the original character of the range rate observations, as described in Eddy & Sutermeister (1975) or in Barthel et al. (1978), which may be for example fringe or doppler counts, nor the effect of non-gravitational and tidal perturbations on the motion of the satellites will be considered in this context.]

Each observed range rate ℓ_i at time t_i is linked to the gravity field of the earth, parameterized by $\underline{\beta} = \underline{\beta}^c + \delta\underline{\beta}$ ($\underline{\beta}^c$ ... known computed longwavelength part of the gravity field, $\delta\underline{\beta}$ ... residual part) through the position and velocity vectors, $\underline{X}$ and $\dot{\underline{X}}$, of the two satellites:

$$\ell_i = \dot{\rho}(t_i; \underline{X}_1(\underline{\beta}), \underline{X}_2(\underline{\beta}), \dot{\underline{X}}_1(\underline{\beta}), \dot{\underline{X}}_2(\underline{\beta})) + \epsilon_i \tag{2}$$

with ϵ_i ... observation error. With $\underline{Y}_1^T = (\underline{X}_1, \dot{\underline{X}}_1)^T$ for the complete state vector and with $\underline{Y}_{10}$ for the state vector at $t = t_0$ (initial condition) a Taylor expansion of equation (2) at the computed reference locations S_1^c and S_2^c of the two satellites yields:

$$\begin{aligned} \ell_i = {} & \dot{\rho}_i^c(t_i; S_1^c, S_2^c) + (\mathrm{grad}_{\underline{Y}_1} \dot{\rho})_i^T (S_1^c)[(\mathrm{grad}_{\underline{Y}_{10}} \underline{Y}_1)^T (S_1^c) \underline{\Delta Y}_{10} + \\ & (\mathrm{grad}_{\underline{\beta}} \underline{Y}_1)^T (S_1^c) \underline{\delta\beta}] + (\mathrm{grad}_{\underline{Y}_2} \dot{\rho})_i^T (S_2^c)[(\mathrm{grad}_{\underline{Y}_{20}} \underline{Y}_2)^T (S_2^c) \underline{\Delta Y}_{20} + \\ & (\mathrm{grad}_{\underline{\beta}} \underline{Y}_1)^T (S_2^c) \underline{\delta\beta}] + \epsilon_i, \end{aligned} \tag{3}$$

where ϵ_i shall now contain, besides the measurement noise, the terms of second and higher order of the series expansion. [The gradient of a vector shall thereby express the gradient of the components the vector and constitute a matrix of dimension (no. of gradient components) x (no. of vector components)]. Equation (1) yields:

$$-(\mathrm{grad}_{\underline{Y}_1} \dot{\rho})(S_1^c) = (\mathrm{grad}_{\underline{Y}_2} \dot{\rho})(S_2^c) = \begin{bmatrix} \rho^{c\,-1} (\dot{\underline{X}}_{12}^c - \dot{\rho}^c \underline{e}_{12}^c) \\ \underline{e}_{12}^c \end{bmatrix},$$

and in analogy to Schwarz (1970) we denote

$$(\mathrm{grad}_{\underline{Y}_{10}}\,\underline{Y}_1)\,(S_1^c) = \underline{\Phi}_1\,,$$

$$(\mathrm{grad}_{\underline{Y}_{20}}\,\underline{Y}_2)\,(S_2^c) = \underline{\Phi}_2\,,$$

$$[\underline{\Phi}_1\,,\,\underline{\Phi}_2\,]^T = \underline{\Phi}^T\,,$$

$$(\mathrm{grad}_{\underline{\beta}}\,\underline{Y}_1)\,(S_1^c) = \underline{W}_1\,,$$

$$(\mathrm{grad}_{\underline{\beta}}\,\underline{Y}_2)\,(S_2^c) = \underline{W}_2\,,$$

$$\underline{W}_2 - \underline{W}_1 = \underline{W}_{12}\,.$$

Then equation (3) becomes

$$\underline{\ell}_i = \dot{\rho}_i^c + \begin{bmatrix} \rho^{c\,-1}\,\underline{C} \\ \underline{e}_{12} \end{bmatrix}_i^T \left[\underline{W}_{12}^T\,\underline{\delta\beta} + \Phi^T \begin{bmatrix} \underline{\Delta Y}_{10} \\ \underline{\Delta Y}_{20} \end{bmatrix} \right] + \epsilon_i \qquad (4)$$

(with $\underline{C} = \dot{\underline{X}}_{12}^c - \dot{\rho}^c\,\underline{e}_{12}^c$, according to Rummel et al. (1978), the cross-track velocity) or as a formal matrix equation

$$\underline{r} = \underline{B}\,\underline{Y} + \underline{A}\,\underline{\delta\beta} + \underline{\epsilon} \qquad (5)$$

where

$$\underline{r} = \underline{\ell} - \underline{\dot{\rho}}^c,\quad \underline{B} = \underline{\begin{bmatrix} \rho^{c-1}\,\underline{C} \\ \underline{e}_{12} \end{bmatrix}^T \Phi^T},\quad \underline{Y} = \begin{bmatrix} \underline{\Delta Y}_{10} \\ \underline{\Delta Y}_{20} \end{bmatrix},\ \text{and}\ \underline{A} = \underline{\begin{bmatrix} \rho^{c\,-1}\,\underline{C} \\ \underline{e}_{12} \end{bmatrix}^T W_{12}^T}.$$

If $\underline{D}$ is the a priori variance covariance matrix of $\underline{r}$ and $\underline{C}_{\beta}$ the second-order moment ("covariance matrix", reproducing kernel) of $\underline{\delta\beta}$ with $\underline{\delta\beta}$ assumed to be an element of an infinite dimensional Hilbert space, then the best linear estimates for $\underline{Y}$ and $\underline{\delta\beta}$ are, see e.g. Moritz (1972):

$$\hat{\underline{Y}} = \begin{bmatrix} \hat{\underline{\Delta Y}}_{10} \\ \hat{\underline{\Delta Y}}_{20} \end{bmatrix} = \left[\underline{\Phi \begin{bmatrix} \rho^{c\,-1}\,\underline{C} \\ \underline{e}_{12} \end{bmatrix}}\,\underline{Q}^{-1}\,\underline{\begin{bmatrix} \rho^{c-1}\,\underline{C} \\ \underline{e}_{12} \end{bmatrix}\Phi^T} \right]^{-1} \underline{\Phi \begin{bmatrix} \rho^{c-1}\,\underline{C} \\ \underline{e}_{12} \end{bmatrix}}\,\underline{Q}^{-1}\,\underline{r} \qquad (6)$$

$$\hat{\underline{\delta\beta}} = \underline{C}_{\beta}\,\underline{W_{12}\begin{bmatrix} \rho^{c-1}\,\underline{C} \\ \underline{e}_{12} \end{bmatrix}}\,\underline{Q}^{-1} \left(\underline{r} - \underline{\begin{bmatrix} \rho^{c\,-1}\,\underline{C} \\ \underline{e}_{12} \end{bmatrix}^T \Phi^T} \begin{bmatrix} \underline{\Delta Y}_{10} \\ \underline{\Delta Y}_{20} \end{bmatrix}, \right) \qquad (7)$$

$$\underline{Q} = \underline{A}\,\underline{C}_{\beta}\,\underline{A}^T + \underline{D} = \underline{\begin{bmatrix} \rho^{c\,-1}\,\underline{C} \\ \underline{e}_{12} \end{bmatrix}^T W_{12}^T}\,\underline{C}_{\beta}\,\underline{W_{12}\begin{bmatrix} \rho^{c\,-1}\,\underline{C} \\ \underline{e}_{12} \end{bmatrix}} + \underline{D} \qquad (8)$$

Problems in using this type of least squares collocation solution come from the difficulties in deriving the matrix $\underline{Q}$ of equation (8). It requires the connection of the mentioned Hilbert space with reproducing kernel (with $\underline{C}_9$ based on a chosen degree variance model) with time dependent functionals such as the state vectors of the two satellites. This conceptual problem and linked to it the problem of the practical computation of Q for instance by numerical or analytical integration will not be investigated in this report. Instead an alternative approach will be analyzed which comes also closer to the concept of "direct gravity mapping" as formulated by Muller & Sjogren (1968).

3. Observational Model for Range Rate Changes and Orbit Requirements

Instead of working with the range rates $\dot{\rho}$ one can also analyze their time derivative $\ddot{\rho}$, the range rate changes. Equation (1) yields:

$$\ddot{\rho}(S_1, S_2) = \underline{X}_{12} \cdot \underline{e}_{12} + \dot{\underline{X}}_{12} \cdot \dot{\underline{e}}_{12} \tag{9}$$

For SST in the high-low mode Hajela (1978, p. 6) showed that the second term on the right-hand side is negligible, a fact that tremendously facilitates the whole model. It is to be shown that this is at least on an average the case for the low-low version, too. With

$$\dot{\underline{X}}_{12} \cdot \dot{\underline{e}}_{12} = \rho_{12}^{-1} \left(\dot{\underline{X}}^2_{12} - \dot{\rho}^2 \right) = \rho_{12}^{-1} \underline{C}^2 .$$

equation (9) becomes

$$\ddot{\rho}(S_1, S_2) = \ddot{\underline{X}}_{12} \cdot \underline{e}_{12} + \rho_{12}^{-1} \underline{C}^2 \tag{10}$$

Introducing the reference range rate change

$$\ddot{\rho}^e_{12} = \ddot{\underline{X}}^c_{12} \cdot \underline{e}_{12} + \rho_{12}^{-1} \underline{C}^{c\,2}$$

as derived from some approximate state vectors and an ellipsoidal reference field or, in addition, a set of known potential coefficients and assuming $\underline{e}_{12}$ and ρ_{12} to be known (which has no consequence on the following evaluations) one obtains as difference:

$$\delta\ddot{\rho} = \underline{\delta\ddot{X}}_{12} \cdot \underline{e}_{12} + \rho_{12}^{-1} \underline{\delta C}^2 . \tag{11}$$

Evaluation of the average magnitude of the second term on the right hand side of equation (11) or of $\rho^{-1} \underline{\delta\dot{X}}^2_{12}$, since

$$\rho_{12}^{-1} \underline{\delta C}^2 < \rho_{12}^{-1} \underline{\delta\dot{X}}^2_{12} :$$

From a linearization of the energy conservation law follows according to Wolff (1969):

$$\underline{\delta\dot{X}}^2_{12} = (\underline{\delta\dot{X}}_2 - \underline{\delta\dot{X}}_1)^2 \doteq \frac{1}{\underline{\dot{X}}^{c2}} T^2_{12},$$

where $\underline{\dot{X}}^c$ is the mean velocity of the satellites and $T_{12} = T(S_2) - T(S_1)$ the disturbing potential difference. The average behavior of the earth's gravity potential is expressed by a chosen degree variance model, with $\sigma^2_\ell(T)$ the disturbing potential degree variances. On an average the second term becomes therefore:

$$\text{ave}(\rho^{-1}_{12}\,\underline{\delta\dot{X}}^2_{12}) = \text{ave}(\frac{1}{\rho_{12}\underline{\dot{X}}^{c2}} T^2) = \frac{1}{\rho_{12}\underline{\dot{X}}^{c2}} (\text{var } T(S_1) + \\ - 2\,\text{cov}(T(S_1), T(S_2)) + \text{var } T(S_2)). \qquad (12)$$

Evaluation of the average magnitude of the first term on the right hand side of equation (11), i.e. of

$$\underline{\delta\ddot{X}}_{12} \cdot \underline{e}_{12}:$$

E.g. for radial separation one obtains

$$\underline{\delta\ddot{X}}_{12} \cdot \underline{e}_{12} = \frac{\partial}{\partial r}(T(S_2) - T(S_1)) = T_{r_{12}},$$

and

$$\text{ave}(\underline{\delta X}_{12} \cdot \underline{e}_{12}) = (\text{var } T_r(S_1) - 2\,\text{cov}(T_r(S_1), T_r(S_2)) + \text{var } T_r(S_2)) \qquad (13)$$

The average magnitude of the two terms on the right hand side of equation (11) for the high low as well as for the low low mode is contained in Table 1. The values have been determined - based on equations (12) and (13) - from equations (A5) and (A6), described in the appendix.

Table 1. Average magnitude of the two terms on the right hand side of equation (11)

mode	wave lengths ℓ	first term of (11) 10^{-5} msec^{-2}	second term of (11) 10^{-6} msec^{-2}
high	2 - ∞	18.068	$0.277 \cdot 10^{-6}$
-low	19 - ∞	5.066	$0.000_7 \cdot 10^{-6}$
low	2 - ∞	1.498	$0.244 \cdot 10^{-6}$
-low	19 - ∞	1.078	$0.016 \cdot 10^{-6}$

The numbers of Table 1 as well as the level of the observational noise, to be discussed later, clearly indicate that the second term can be neglected without significant loss of accuracy. The basic model will therefore be:

$$\ddot{\rho}(S_1, S_2) \doteq \underline{\ddot{X}}_{12} \cdot \underline{e}_{12} \tag{14}$$

From now on, range rate changes are considered as being observed. They are obtained from range rates by numerical differentiation, as discussed e.g. in Rummel et al. (1976) and Hajela (1978). The mathematical model of equation (14) is linked to the observed range rate changes by

$$\ell_i = \ddot{\rho}(t_i; \underline{X}_1(\underline{\beta}), \underline{X}_2(\underline{\beta}), \underline{\ddot{X}}_1(\underline{\beta}), \underline{\ddot{X}}_2(\underline{\beta})) + \epsilon_i \tag{15}$$

Assuming for a moment the positions S_1 and S_2 of the two satellites to be known, the dependence on the unknown gravity parameters $\underline{\delta\beta} = \underline{\beta} - \underline{\beta}^c$ is expressed by

$$\ell_i = \ddot{\rho}_i^c(t_i; S_1, S_2) + \underline{\delta\ddot{X}}_{12} \cdot \underline{e}_{12} + \epsilon_i ,$$

and since

$$\underline{\delta\ddot{X}}_{12} = \delta\ddot{X}_2 - \delta\ddot{X}_1 = (\mathrm{grad}_{\underline{X}_2} T)(S_2) - (\mathrm{grad}_{\underline{X}_1} T)(S_1)$$

$$= \mathrm{grad}\, T_{12} ,$$

the observation equation becomes in vector form:

$$\underline{\ell} = \ddot{\rho}^c(t_i; S_1, S_2) + \underline{(\mathrm{grad}_{\delta\beta}(\mathrm{grad}\, T_{12}))^T (S_1, S_2)\, \delta\beta} \cdot \underline{e}_{12}^c + \underline{\epsilon} . \tag{16}$$

In analogy to the last chapter the uncertainty of the satellite positions is taken care of by

$$\underline{\ell} = \ddot{\rho}^c(t_i; S_1^c, S_2^c) + \underline{(\mathrm{grad}_{\underline{X}_1} \ddot{\rho})^T (S_1^c)\, \Delta\underline{X}_1} + \underline{(\mathrm{grad}_{\underline{X}_2} \ddot{\rho})^T (S_2^c)\, \Delta\underline{X}_2}$$

$$+ \underline{(\mathrm{grad}_{\delta\beta}(\mathrm{grad}\, T_{12}))^T (S_1^c, S_2^c)\, \delta\beta} \cdot \underline{e}_{12}^c + \underline{\epsilon} \tag{17}$$

The terms $(\mathrm{grad}_{\underline{X}_1} \ddot{\rho})^T (S_1^c)$ and $(\mathrm{grad}_{\underline{X}_2} \ddot{\rho})^T (S_2^c)$ express on one hand the coefficients for an orbital improvement from the observed range rate changes, on the other hand they define the sensitivity of the observations on orbit errors as expressed by $\Delta\underline{X}$, the difference between the actual and the reference orbit. This type of coefficient matrix is denoted $\underline{\Omega}$:

$$\underline{\Omega} = (\mathrm{grad}_{\underline{X}_1} \ddot{\rho})^T (S_1^c) = [-\rho^{c\,-1} (\underline{\ddot{X}}_{12} - \ddot{\rho}\, \underline{e}_{12}^c) + [\frac{\partial^2 V}{\partial X_i \partial X_j}]\, e_{12}^c \,] \quad i, j = 1, 2, 3$$

Expressing Ω in a local (ζ, ξ, η)-system as defined in Reed (1973) and assuming radial separation of the two satellites, it becomes

$$\underline{\Omega} = -\rho^{c-1}\left(\nabla V_{12} - \ddot{\rho}^{c}\begin{pmatrix} e_{12} \\ 0 \\ 0 \end{pmatrix}\right) + \begin{pmatrix} V_{12}^{\zeta\zeta} \\ V_{12}^{\zeta\xi} \\ V_{12}^{\zeta\eta} \end{pmatrix} < -\rho^{-1}\begin{pmatrix} V_{12}^{\zeta} \\ V_{12}^{\xi} \\ V_{12}^{\eta} \end{pmatrix} + \begin{pmatrix} V_{12}^{\zeta\zeta} \\ V_{12}^{\zeta\xi} \\ V_{12}^{\zeta\eta} \end{pmatrix},$$

where e.g. $V_{12}^{\zeta\zeta}$ stands for $\frac{\partial^2 V_2}{\partial\zeta\,\partial\zeta} - \frac{\partial^2 V_1}{\partial\zeta\,\partial\zeta}$.

$\underline{\Omega}$ is now split into the contribution of the normal field, Ω_n and into the average contribution of the residual field, Ω_r, i.e.:

$$\underline{\Omega} = \underline{\Omega}_n + \underline{\Omega}_r \qquad \text{and}$$

$$\underline{\Omega}_n = -\rho^{-1}\begin{pmatrix} \Gamma_{12}^{\zeta} \\ \Gamma_{12}^{\xi} \\ \Gamma_{12}^{\eta} \end{pmatrix} + \begin{pmatrix} \Gamma_{12}^{\zeta\zeta} \\ \Gamma_{12}^{\zeta\xi} \\ \Gamma_{12}^{\zeta\eta} \end{pmatrix},$$

$$\underline{\Omega}_r = \text{ave}\left(-\rho^{-1}\begin{pmatrix} T_{12}^{\zeta} \\ T_{12}^{\xi} \\ T_{12}^{\eta} \end{pmatrix}\right) + \text{ave}\begin{pmatrix} T_{12}^{\zeta\zeta} \\ T_{12}^{\zeta\xi} \\ T_{12}^{\zeta\eta} \end{pmatrix}.$$

Magnitude of $\underline{\Omega}_n$

The Γ-terms for the determination of $\underline{\Omega}_n$ are (Heiskanen and Moritz, 1967, p. 231):

$$\Gamma^{\zeta} = -\frac{GM}{r^2}\left[1 - \sum_{\ell=1}^{2}(2\ell+1)\,J_{2\ell}\left(\frac{a}{r}\right)^{2\ell} P_{2\ell}(\sin\varphi)\right],$$

$$\Gamma^{\xi} = -\frac{GM}{r^2}\sum_{\ell=1}^{2} J_{2\ell}\left(\frac{a}{r}\right)^{2\ell}\frac{dP_{2\ell}}{d\varphi},$$

$$\Gamma^{\eta} = 0,$$

with GM ... geocentric gravitational constant
$J_{2\ell}$ ... spherical harmonic coefficients
a ... semimajor axis of the earth
$P_{2\ell}(\cos\varphi)$ ... Legendre polynomial.

Inserting the geodetic constants of the Geodetic Reference System, 1967 and assuming a radial separation of 50 km at 200 km altitude one obtains at most:

$$\underline{\Omega}_n = \begin{cases} -0.272 \cdot 10^{-6}\ \mathrm{sec}^{-2} & \text{radial} \quad (\varphi = 0^\circ) \\ 0.000\,84 \cdot 10^{-5}\ \mathrm{sec}^{-2} & \text{latitudinal} \quad (\varphi = 45^\circ) \\ 0 & \text{longitudinal} \end{cases}$$

For an along or cross track separation all three components are less than 1 E.U. = 10^{-9} sec^{-2} which is obvious because of the distinct dominance of the radial term in the reference field.

Magnitude of $\underline{\Omega}_r$

The average values for T_{12}^{ζ} and $T_{12}^{\zeta\zeta}$ are again taken from an adopted degree variance model. Equations (A6) and (A7) of the appendix yield

$$\Omega_r^{\zeta} = \text{ave}\,(-\rho^{-1} T_{12}^{\zeta}) + \text{ave}\, T_{12}^{\zeta\zeta} = 0.63 \text{ E.U.}$$

The two other components will on the average be at most of the same magnitude.

The entire contribution, $\delta\ddot{\rho}$, of an orbit error $\underline{\Delta X}_1$ or $\underline{\Delta x}_1$ if expressed in the (ζ, ξ, η)-system is:

$$\delta\ddot{o} = (\underline{\Omega}_n + \underline{\Omega}_r)^T \underline{\Delta x} .$$

The orbit corrections $\underline{\Delta X}_1$ and $\underline{\Delta X}_2$ depend on the gravity parameters $\underline{\delta\beta}$ (short wavelength part) and on the initial state vector corrections $\underline{\Delta X}_{10}$ and $\underline{\Delta X}_{20}$ (long wavelength part) and so does $\underline{\Delta x}$. Of concern for the gravity parameter estimation are unmodelled short wavelength effects. They are caused especially by non-gravitational disturbances, and to a less extent (because of the long-wavelength characteristic) by tracking error and tracking station uncertainties. The latter when multiplied with short-wavelength coefficients, i.e. with $\underline{\Omega}_r$, may cause problems, too. In figure 1 the magnitude of the range rate change error due to an orbit error for the terms Ω_r^{ζ} (radial), Ω_n^{ξ} (along or cross track), and Ω_r^{ζ} ($\doteq \Omega_r^{\xi} \doteq \Omega_r^{\eta}$) are shown. It clearly indicates that especially the disturbances in the radial component of the orbit are critical. There are also given three levels of measurement precision (0.001, 0.01, and 0.1 mgal). Their relation to what is actually feasible will be given later.

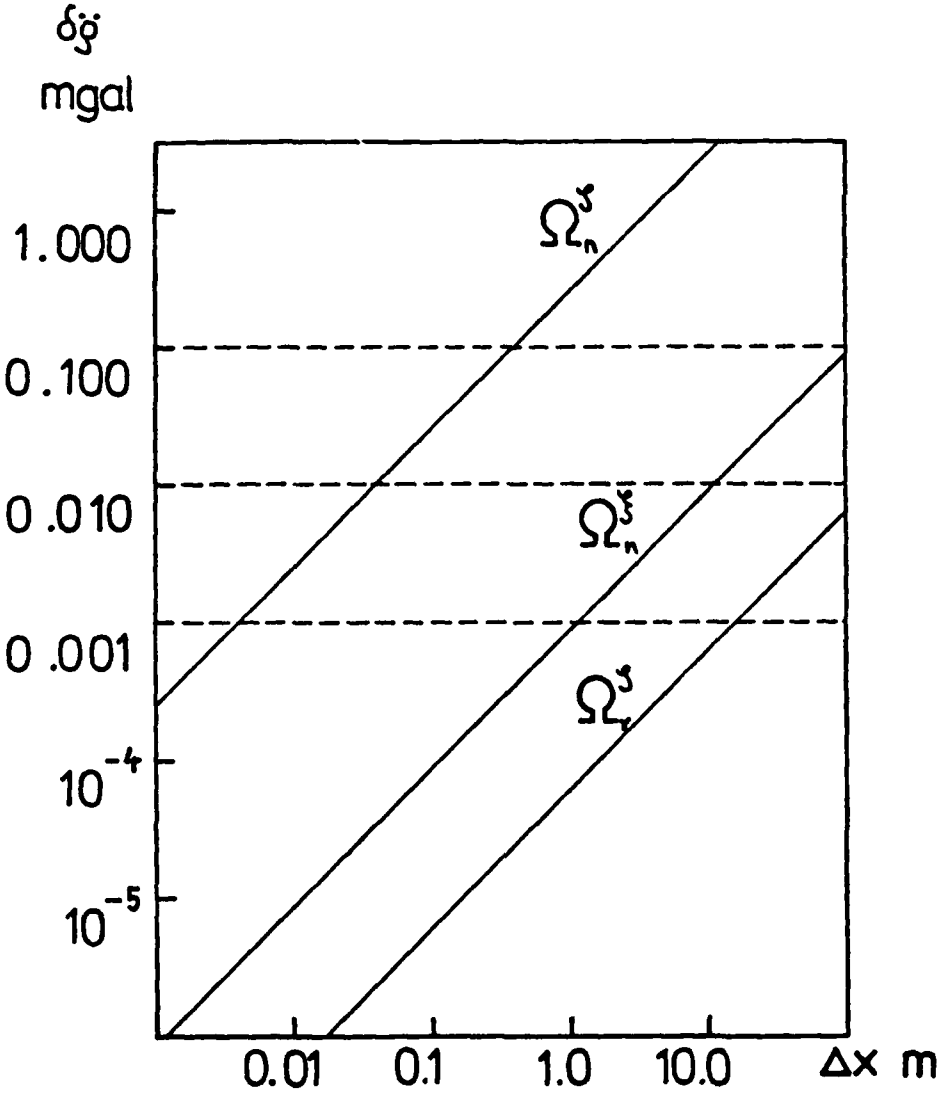

Figure 1. Range rate change error due to an orbit error for the terms Ω_n^{ζ} (radial), Ω_n^{ξ} (along or cross track), and Ω_r^{ζ} ($\doteq \Omega_r^{\xi} \doteq \Omega_r^{\eta}$).

In the following - after having some insight into the impact of errors on the orbit - the orbital correction will be disregarded. From equation (17) the estimation model becomes therefore:

$$\ell = \ddot{\rho}^c(t_1; S_1, S_2) + \underline{(\mathrm{grad}_{\delta\beta}\ (\mathrm{grad}\ T_{12}))^T\ (S_1, S_2)\ \delta\beta \cdot e_{12}} + \underline{\epsilon} \qquad (18)$$

or with

$$\underline{r} = \underline{\ell} - \underline{\ddot{o}}^{c}(t_i ; S_1, S_2), \text{ and } \underline{A} = \underline{(\text{grad}_{\delta\beta}(\text{grad } T_{12}))^{T}}\ (S_1, S_2):$$

$$\underline{r} = \underline{A}\ \underline{\delta\beta} + \underline{\epsilon} \tag{19}$$

With $\underline{D}$ now the a priori variance covariance matrix of the range rate changes $\underline{r}$ and $\underline{C}_{\beta}$ as before the best linear estimate of

$$\min\left(\|\underline{r} - \underline{A}\ \underline{\delta\beta}\|^2_{\underline{D}^{-1}} + \|\underline{\delta\beta}\|^2_{\underline{C}_{\beta}^{-1}} \right), \tag{20}$$

becomes

$$\begin{aligned} \underline{\delta\beta} &= (\underline{A}^{T}\ \underline{D}^{-1}\ \underline{A} + \underline{C}_{\beta}^{-1})^{-1}\ \underline{A}^{T}\ \underline{D}^{-1}\ \underline{r} \\ &= \underline{C}_{\beta}\ \underline{A}^{T}\ (\underline{A}\ \underline{C}_{\beta}\ \underline{A}^{T} + \underline{D})^{-1}\ \underline{r} \\ &= \underline{L}\ \underline{r} \end{aligned} \tag{21}$$

where $\underline{L} = \underline{C}_{\beta}\ \underline{A}^{T}\ (\underline{A}\ \underline{C}_{\beta}\ \underline{A}^{T} + \underline{D})^{-1}$ is the estimator.

4. Computational Procedure and Error Measure

The goal of this study is to perform an error analysis of SST in the low-low mode. The adequate error measure is the a posteriori variance-covariance matrix for the gravity parameters to be estimated from a realistical arrangement of sample points. The a posteriori variance-covariance matrix provides on one hand a reliable measure of the variance of the quantities to be estimated and on the other hand the covariance structure, too, which shows how independent the estimates actually are. The commonly used form of the a posteriori variance-covariance matrix, derived from equation (21), is:

$$\underline{E}_{\beta} = \underline{C}_{\beta} - \underline{C}_{\beta}\ \underline{A}^{T}\ (\underline{A}\ \underline{C}_{\beta}\ \underline{A}^{T} + \underline{D})^{-1}\ \underline{A}\ \underline{C}_{\beta}\,. \tag{22}$$

$\underline{E}_{\beta}$ is the second-order moment $E\{[\hat{\underline{\delta\beta}} - \underline{\delta\beta}][\hat{\underline{\delta\beta}} - \underline{\delta\beta}]^{T}\}$. With model equation (19) and the estimate (21) one finds

$$\begin{aligned} E\{[\hat{\underline{\delta\beta}} - \underline{\delta\beta}][\hat{\underline{\delta\beta}} - \underline{\delta\beta}]^{T}\} &= E\{[\underline{L}\ (\underline{A}\ \underline{\delta\beta} + \underline{\epsilon}) - \underline{\delta\beta}][\underline{L}\ (\underline{A}\ \underline{\delta\beta} + \underline{\epsilon}) - \underline{\delta\beta}]^{T}\} \\ &= \underline{B}\ E\{\underline{\delta\beta}\ \underline{\delta\beta}^{T}\}\ \underline{B}^{T} + \underline{L}\ \underline{D}\ \underline{L}^{T}, \end{aligned}$$

where $B = (\underline{L}\ \underline{A} - \underline{I})$, $\underline{I}$... identity matrix, and $E\{\epsilon\} = 0$. The expectation operator has to be replaced by the averaging operator, M, over the sphere, see e.g. Heiskanen and Moritz (1967, p.258) to obtain

$$\underline{E}_{\beta} = \underline{B}\,\underline{C}_{\beta}\,\underline{B}^{T} + \underline{L}\,\underline{D}\,\underline{L}^{T} \tag{23}$$

This is an alternative formulation of equation (22). It presents with the first term, $\underline{B}\,\underline{C}_{\beta}\,\underline{B}^{T}$, the configuration inadequacy; $\underline{B} = \underline{L}\,\underline{A} - \underline{I}$ would be 0 in the optimal case. The second term shows the propagation of the measurement error. Thus the contribution of the first term could be minimized by optimizing the configuration, that of the second term mainly by improving the observational precision.

In equation (22) $\underline{A}\,\underline{C}_{\beta}\,\underline{A}^{T}$ is nothing but $\underline{C}_{\ddot{\rho}}$, the a priori variance covariance matrix of the observations, and $\underline{C}_{\beta}\,\underline{A}^{T}$ the cross-covariance $\underline{C}_{\beta\ddot{\rho}}$ between the parameters to be estimated and the range rate changes, or:

$$\underline{E}_{\beta} = \underline{C}_{\beta} - \underline{C}_{\beta\ddot{\rho}}(\underline{C}_{\ddot{\rho}} + \underline{D})^{-1}\,\underline{C}_{\beta\ddot{\rho}}^{T} \tag{24}$$

Since from equation (14)

$$\ddot{\rho} = (\ddot{\underline{X}}_2 - \ddot{\underline{X}}_1)\cdot\underline{e}_{12} = (\nabla T_2 - \nabla T_1)\cdot\underline{e}_{12}$$

where T will be referred to a known reference field up to degree $\ell_{max} = 12$, a single matrix element, $[ij]$, of $\underline{C}_{\ddot{\rho}}$ becomes

$$\begin{aligned} C_{\ddot{\rho},ij} &= \underline{e}_{12,i}^{T}\, C\{(\nabla T_2 - \nabla T_1)_i ;\ (\nabla T_2 - \nabla T_1)_j\}\ \underline{e}_{12,j} \\ &= \underline{e}_{12,i}^{T}\,[C\{\nabla T_{2,i};\nabla T_{2,j}\} - C\{\nabla T_{2,i};\nabla T_{1,j}\} - C\{\nabla T_{1,i};\nabla T_{2,j}\} \\ &\qquad + C\{\nabla T_{1,i};\nabla T_{1,j}\}]\ \underline{e}_{12,j}\ . \end{aligned} \tag{25}$$

The gradient is given in an earth-fixed (r, φ, λ)-system with

$$\nabla T = \left[\frac{\partial T}{\partial r}, \frac{1}{r}\frac{\partial T}{\partial \varphi}, \frac{1}{r\cos\varphi}\frac{\partial T}{\partial \lambda}\right]^{T}$$

Thus, before inserted into (25) the unit vectors $\underline{e}_{12}$ provided in an earth-fixed (x, y, z)-system have to be transformed to the (r, φ, λ)-system (see Hajela, 1978, p. 8) by

$$\underline{e}_{12}^{(r,\varphi,\lambda)} = \underline{\psi}\ \underline{e}_{12}^{(x,y,z)} \quad \text{and}$$

$$\underline{\psi} = \begin{bmatrix} \cos\varphi\cos\lambda & \cos\varphi\sin\lambda & \sin\varphi \\ -\sin\varphi\cos\lambda & \sin\varphi\sin\lambda & \cos\varphi \\ -\sin\lambda & \cos\lambda & \end{bmatrix}$$

Similarily an element of $\underline{C}_{\beta\ddot{\rho}}$ becomes:

$$C_{\beta\ddot{\rho},j} = [C\{\delta\beta, \nabla T_{2,j}\} - C\{\delta\beta, \nabla T_{1,j}\}]^{T}\ \underline{e}_{12,j}\ . \tag{26}$$

The subroutine COVAX described in Tscherning (1976) provides all needed covariance elements. Instead of the gradient elements $\left(\frac{\partial T}{\partial r}, \frac{1}{r}\frac{\partial T}{\partial \varphi}, \frac{1}{r\cos\varphi}\frac{\partial T}{\partial \lambda}\right)$ e.g. in units of mgal [$= 10^{-5}$ msec^{-2}], it gives $\left(-\frac{1}{r}\frac{\partial T}{\partial r}, -\frac{1}{\gamma r}\frac{\partial T}{\partial \varphi}, -\frac{1}{\gamma r\cos\varphi}\frac{\partial T}{\partial \lambda}\right)$ in units of (E.U., arcsec, arcsec), with γ ... normal gravity. The conversion is carried out by means of the diagonal matrix

$$\begin{bmatrix} -r\,10^{4} & 0 & 0 \\ 0 & -(\gamma/\rho^{sec}) & 0 \\ 0 & 0 & -(\gamma/\rho^{sec}) \end{bmatrix}.$$

The underlying degree variance model used in all computations is (see Tscherning and Rapp, 1974):

$$\sigma_\ell = \frac{425.28\,(\ell-1)}{(\ell-2)(\ell+24)}\ [\text{mgal}^2]$$

for the gravity anomaly degree variance, and

$$r_s = 6.369\,779\,8 \cdot 10^{6}\ \text{m}$$

for the radius of the Bjerhammar sphere. The computation of one single element of $\underline{C}_{\ddot{\rho}}$ requires 6 x 4 different covariance elements and is therefore very time consuming.

As an alternative we used therefore the subroutine COVAPP of Sünkel (1979). This subroutine computes the covariance elements by a spline interpolation from elements stored once for all in a table. The access is organized almost identical to COVAX. For a sufficiently dense interpolation table both subroutines yield almost identical results. COVAPP is much faster than COVAX but requires, of course, additional core storage.

As described in the introduction the gravity parameters investigated in the error analysis will be

- geoid heights and geoid height differences, and
- 1° x 1° mean gravity anomalies (which contain, roughly, information down to a half-wavelength of 100 km).

The estimates for mean gravity anomalies are obtained by averaging over 81 point estimates in each 1° x 1° block.

It remains to define the a priori variance covariance matrix D of the observations. In a real world experiment one could depart from the original range rate observations and derive from them range rate changes by numerical differentiation, as described in Rapp and Hajela (1979). Since we are going to work directly with range rate changes we have to define precision levels for them which correspond in a well defined manner to range rate precisions. We define that certain range rate and range rate precisions correspond to each other if the same piece

of information, e.g. mean gravity anomalies with approximately the same standard deviation and the same resolution can be derived from them. In order to deduce the equivalent precision levels the degree variance model of one observed quantity, e.g. range rate changes equation (A6), is compared with the corresponding degree variance model of the observation noise. The resolution of the measurement process is then defined by that frequency at which the signal, represented by the degree variance model, is equal to the noise in amplitude. For higher frequencies the noise would dominate the signal. In order to have the same resolution for the observation type to be compared with, e.g. range rates, the signal-to-noise ratio has also to be equal to one at this "resolution frequency". Under this assumption one can deduce from the degree variance model of the signal and noise of the second process - equations (A5) and (A9) - the corresponding precision of the second process. Based on the expressions for the degree variance models of signal and noise for range rate and range rate change - derived in the Appendix - figure 2 is computed. The graph relates range rate and range rate change (= acceleration in the line of sight) precisions, covers a range from an altitude of 150 km to 300 km of the satellite system, and is valid for low-low and high-low configurations.

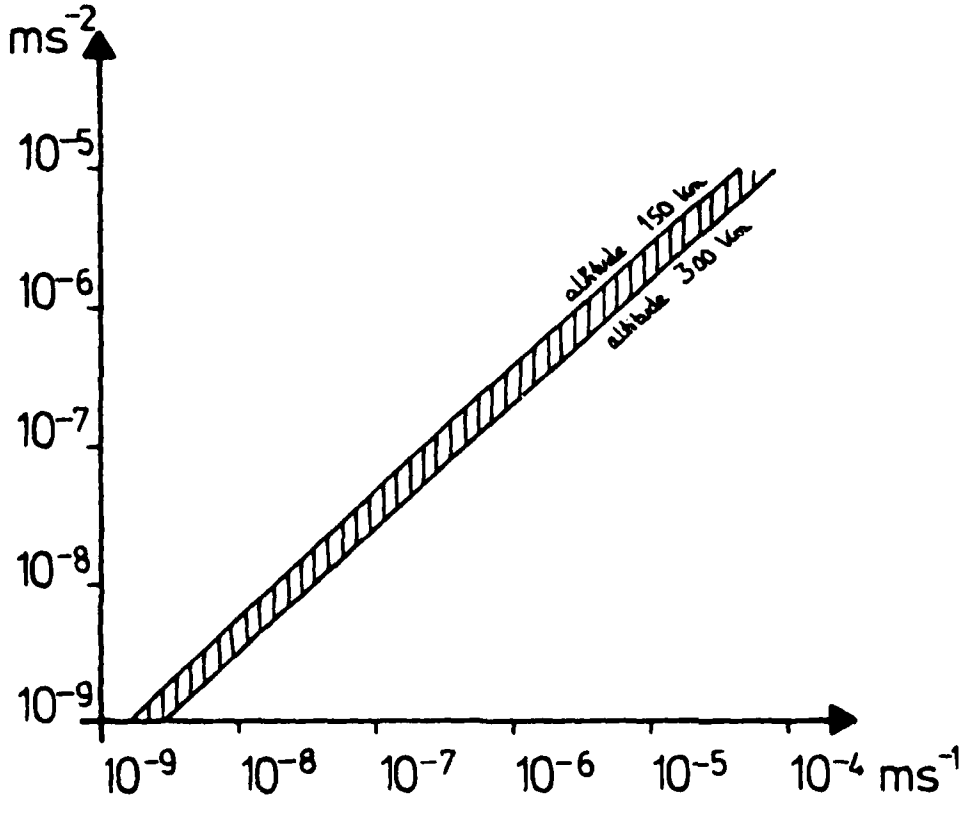

Figure 2. Range rate change (acceleration in the line of sight) precision versus range rate precision.

Figure 2 enables us to assign to each range rate precision introduced into the a priori variance covariance matrix D the equivalent precision for observed range rates. The observations are assumed to be uncorrelated and of equal variance σ_0^2, or $D = \sigma_0^2 \underline{I}$. Representative range rate precisions which are envisaged for coming experiments and the equivalent precision for range rate changes are e.g. :

$$\begin{aligned} 10^{-4}\ \mathrm{ms}^{-1} &\triangleq 1.5 \cdot 10^{-5}\ \mathrm{ms}^{-2} \\ 10^{-5}\ \mathrm{ms}^{-1} &\triangleq 2.2 \cdot 10^{-6}\ \mathrm{ms}^{-2} \\ 10^{-6}\ \mathrm{ms}^{-1} &\triangleq 3.1 \cdot 10^{-7}\ \mathrm{ms}^{-2} \\ 10^{-7}\ \mathrm{ms}^{-1} &\triangleq 4.0 \cdot 10^{-8}\ \mathrm{ms}^{-2} \end{aligned}$$

These numbers allow now to valuate the magnitude of the second term of equation (11) (see table 1), and the impact of systematic and random errors in the orbit as displayed in figure 1.

For numerical simplicity $\underline{C}_{\ddot{\rho}}$ in equation (24) is decomposed into its eigenvalues:

$$\underline{C}_{\ddot{\rho}} = \underline{U}\,\underline{\Lambda}\,\underline{U}^T \tag{27}$$

($\underline{U}$ ... matrix if eigenvectors of $\underline{C}_{\ddot{\rho}}$ with $\underline{U}\,\underline{U}^T = \underline{U}^T\underline{U} = \underline{I}$, and $\underline{\Lambda}$ ... diagonal matrix containing the eigenvalues λ_i). As discussed in Rummel et al. (1979) this allows on one hand the repetition of the error analysis with various observation noise levels σ_0^2 with solving the system of linear equations (27) only once and gives on the other hand a perfect insight into its stability behavior.

Equation (24) becomes then:

$$\underline{E}_{\beta} = \underline{C}_{\beta} - \underline{C}_{\beta\ddot{\rho}}\,\underline{U}\,(\underline{\Lambda} + \sigma_0^2\,\underline{I})^{-1}\,\underline{U}\;\underline{C}_{\beta\ddot{\rho}}$$

or with $\underline{C}_{\beta\ddot{\rho}}\,\underline{U} = \underline{V}$:

$$\underline{E}_{\beta} = \underline{C}_{\beta} - \underline{V}\,(\underline{\Lambda} + \sigma_0^2\,\underline{I})^{-1}\,\underline{V}^T, \tag{28}$$

where $(\underline{\Lambda} + \sigma_0^2\,\underline{I})^{-1}$ is a diagonal matrix with elements $1/(\lambda_i + \sigma_0^2)$. For a separation of the contributions of $\underline{B}\,\underline{C}_{\beta}\,\underline{B}^T$ and $\underline{L}\,\underline{D}\,\underline{L}^T$ of $\underline{E}_{\beta}$ in equation (23) the decomposition is also performed for $\underline{L}\,\underline{D}\,\underline{L}^T$:

$$\begin{aligned} \underline{L}\,\underline{D}\,\underline{L}^T &= \underline{C}_{\beta\ddot{\rho}}\,(\underline{C}_{\ddot{\rho}} + \sigma_0^2\,\underline{I})^{-1}\;\sigma_0^2\,\underline{I}\,(\underline{C}_{\ddot{\rho}} + \sigma_0^2\,\underline{I})^{-1}\,\underline{C}_{\beta\ddot{\rho}}^T \\ &= \underline{V}\,(\underline{\Lambda} + \sigma_0^2\,\underline{I})^{-1}\;\sigma_0^2\,\underline{I}\,(\underline{\Lambda} + \sigma_0^2\,\underline{I})^{-1}\,\underline{V}^T\,. \end{aligned} \tag{29}$$

Finally, it is necessary to generate sample points for the two satellites. A circular orbit has been generated with the following characteristics:

mission period	50 days
inclination	68°
sampling interval	20 sec
altitude of S_1	200 km (and 150 km, 250 km, 300 km)
period	5301 sec

For stability reasons spherical distances of smaller than 0.3° between two adjacent sample points were not permitted. The area for which sample points are used in the analysis is $[\lambda \mid 0° \leq \lambda \leq 5°]$ and $[\varphi \mid 1° \leq \varphi \leq 9°]$. The resulting ground track coverage is given in figure 3.

Figure 3 also contains the six 1° x 1° blocks for which the mean gravity anomaly error analysis will be performed. In order to pronounce the special features of a radial, along track, or cross track arrangement of the two satellites the second satellite is kept exactly in one of these modes throughout the entire mission period for each run to be analyzed.

Figure 3. Ground tracks with sample points and six 1° x 1° blocks for the mean gravity anomaly estimation.

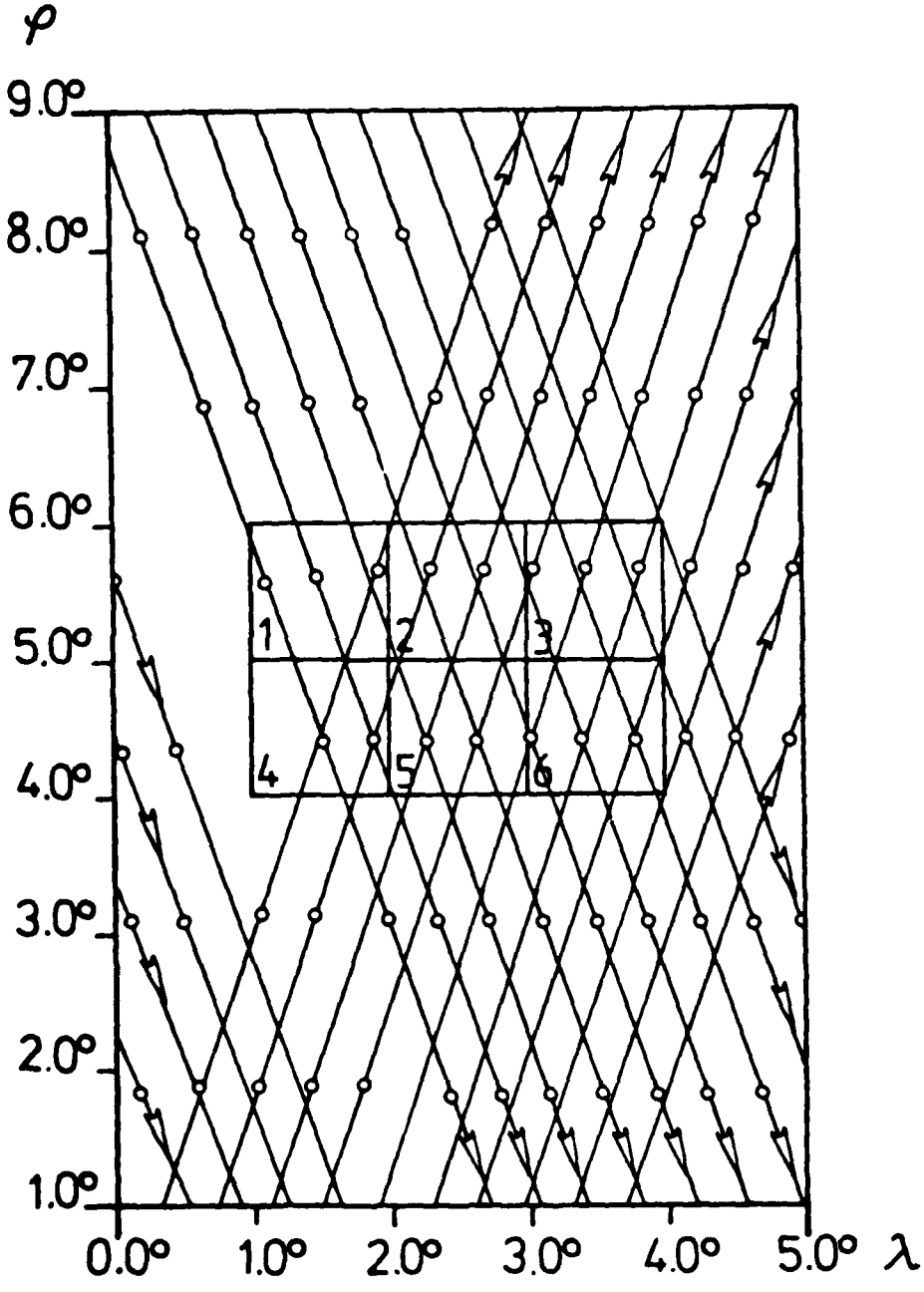

5. Results

All a posteriori standard deviations for mean gravity anomalies, geoid heights, and geoid height differences will refer to a reference field of degree and order 12, assumed to be known.

1°x 1° Mean Gravity Anomalies

Figure 4 shows the standard deviation of an estimated 1°x 1° mean gravity anomaly (block no. 2 in figure 2) computed from the 74 sample points given in figure 2 as a function of the assumed range rate change observational precision $\sigma(\ddot{\rho})$. The corresponding range rate standard deviation is also indicated. The graphs are given for a cross track, along track, and radial separation of 250 km of the two satellites at an altitude of 200 km.

The attainable accuracy of ± 7.5 mgal for a radial separation is much better than that derived from an along track separation which is again better than that of a cross track separation. At a first glance this result surprises. The structure of the gravity field in radial direction should be not much different from that in horizontal direction. For instance the degree variance $\sigma_\ell^2(\delta_r)$ of the radial component of the gradient of the disturbing potential relates to that of the horizontal components $\sigma_\ell^2(\delta_\ell)$ or $\sigma^2(\delta_s)$ (longitudinal and transversal), see equations (A3) and (A4) of the appendix:

$$\sigma_\ell^2(\delta_r) = 2\,\frac{\ell+1}{\ell}\begin{Bmatrix}\sigma_\ell^2(\delta_\ell)\\ \sigma_\ell^2(\delta_s)\end{Bmatrix} \doteq 2\begin{Bmatrix}\sigma_\ell^2(\delta_\ell)\\ \sigma_\ell^2(\delta_s)\end{Bmatrix} \quad \text{for } \ell > 12.$$

The contribution of the pure error propagation part - $\underline{L}\,\underline{D}\,\underline{L}^T$ of equation (23) - also contained in figure 4 is the same for all three types of separation and almost as low as the theoretical lower bound discussed in Rummel (1978). Thus the worse results for along and cross track have to be caused by a configuration problem. The correlation functions for acceleration differences at an altitude of 200 km - figures 5a and 5b - and for the cross-covariance between a surface gravity anomaly and acceleration differences - figures 6a and 6b -, both for separations of 10 km and of 250 km provide an answer: The area covered by observations - see figure 2 - has only an extension of 8°x 5°. But whereas the correlation functions for radial separation have a zero at approximately 5° and little power at spherical distances greater than 5° this is not at all the case for along track separation and even worse for cross track separation. Thus, the spatial arrangement of the two satellites does not principally influence the results of the gravity parameter estimation. For an along track or cross track arrangement only a larger area around the estimation points has to be covered by observations to yield results of the same quality as obtained for radial separation.

Figure 4. Estimated a posteriori standard deviation of a $1° \times 1°$ mean gravity anomaly as a function of the a priori range rate change or range rate precision in dependence of the spatial arrangement of the two satellites (altitude: 200 km; separation: 250 km) and the contribution of $\underline{L}\,\underline{D}\,\underline{L}^T$ (equ. (23)).

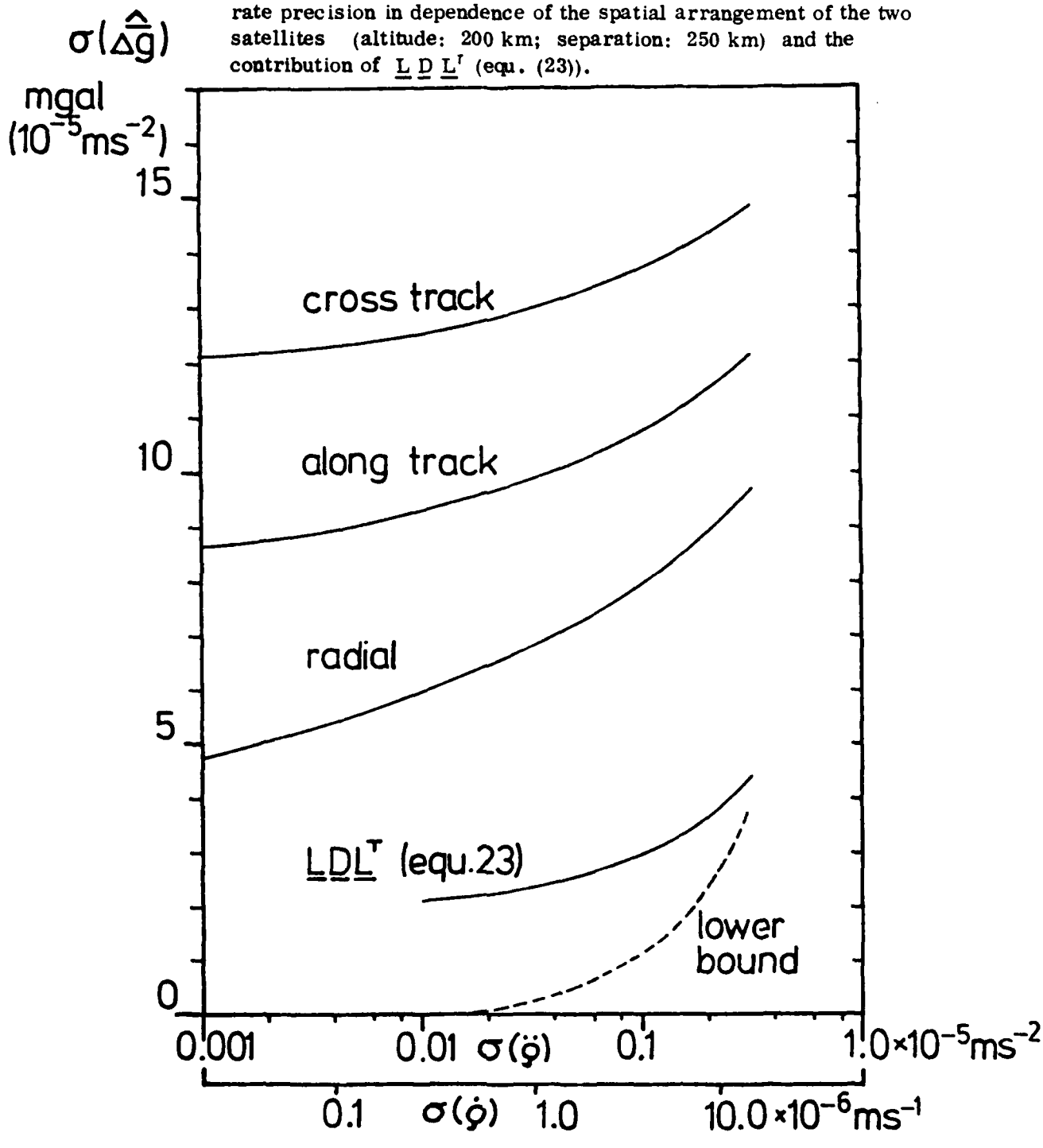

Figure 5a. Covariance function of acceleration differences for a satellite altitude of 200 km and a separation of 250 km (P_1 with $\varphi = 0°$ and $\lambda = 0°$; P_2 with $\varphi = \psi$ and $\lambda = 0°$).

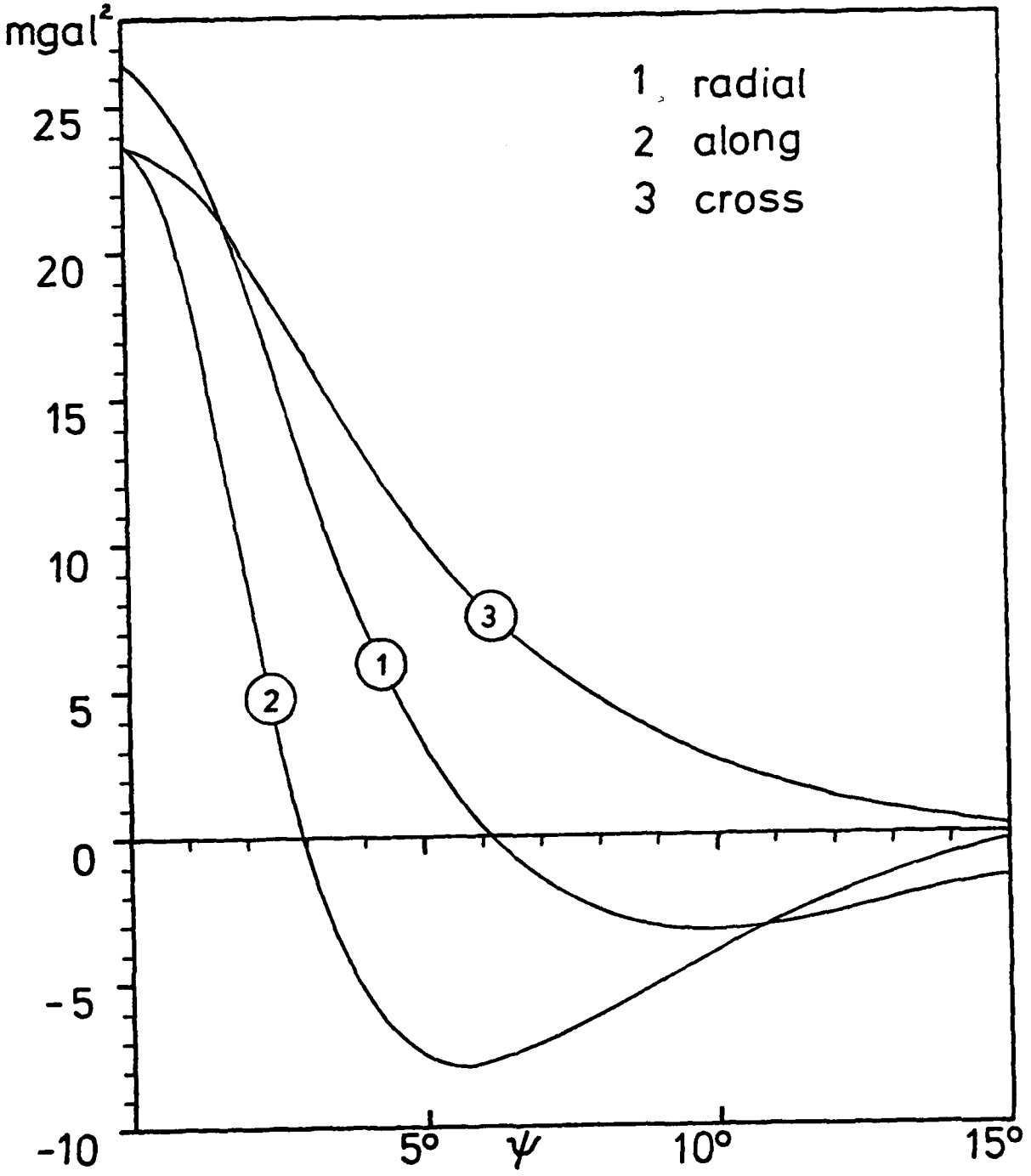

Figure 5b. Covariance function of acceleration differences for a satellite altitude of 200 km and a separation of 10 km (P_1 with $\varphi = 0°$ and $\lambda = 0°$; P_2 with $\varphi = \psi$ and $\lambda = 0°$).

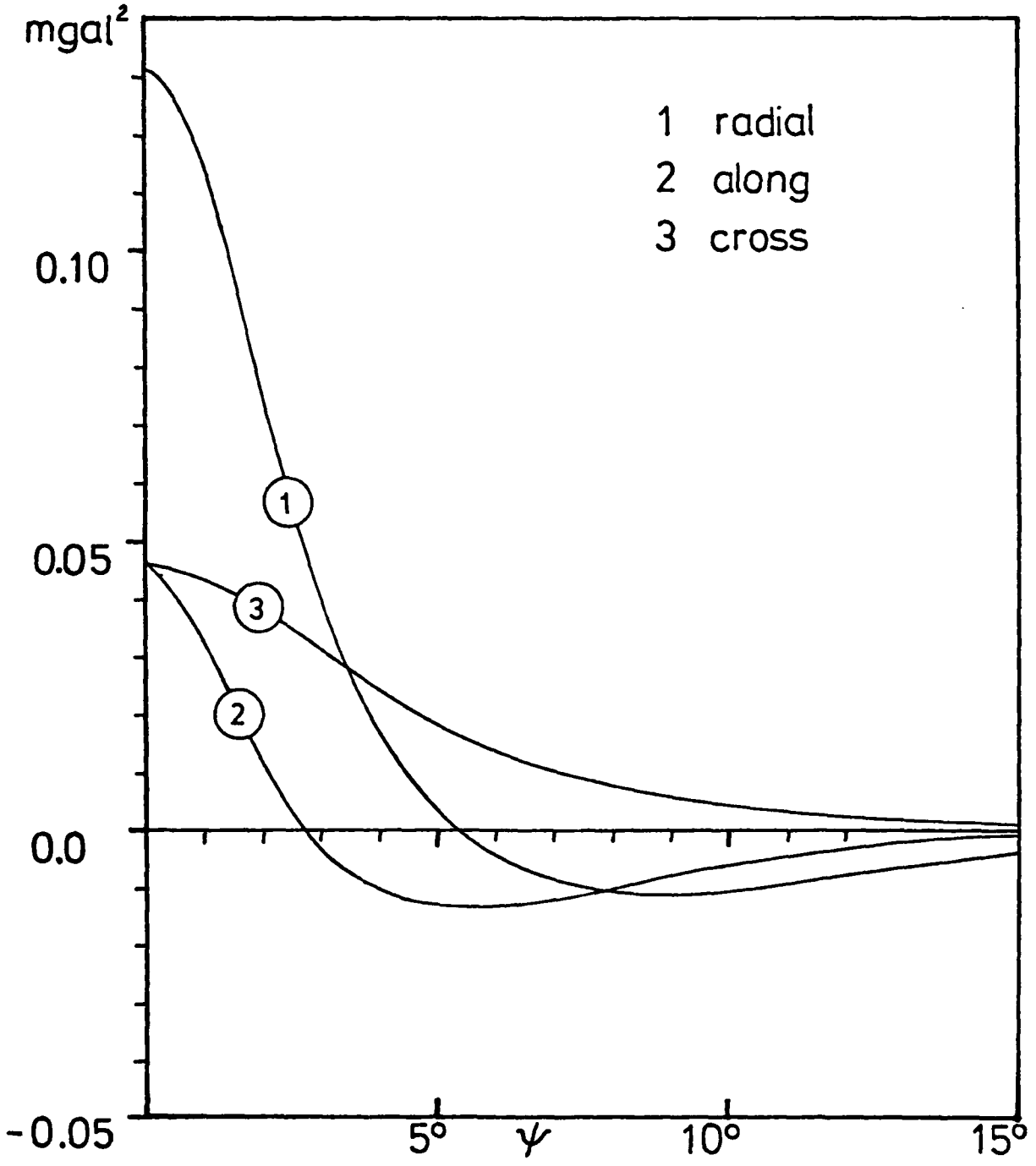

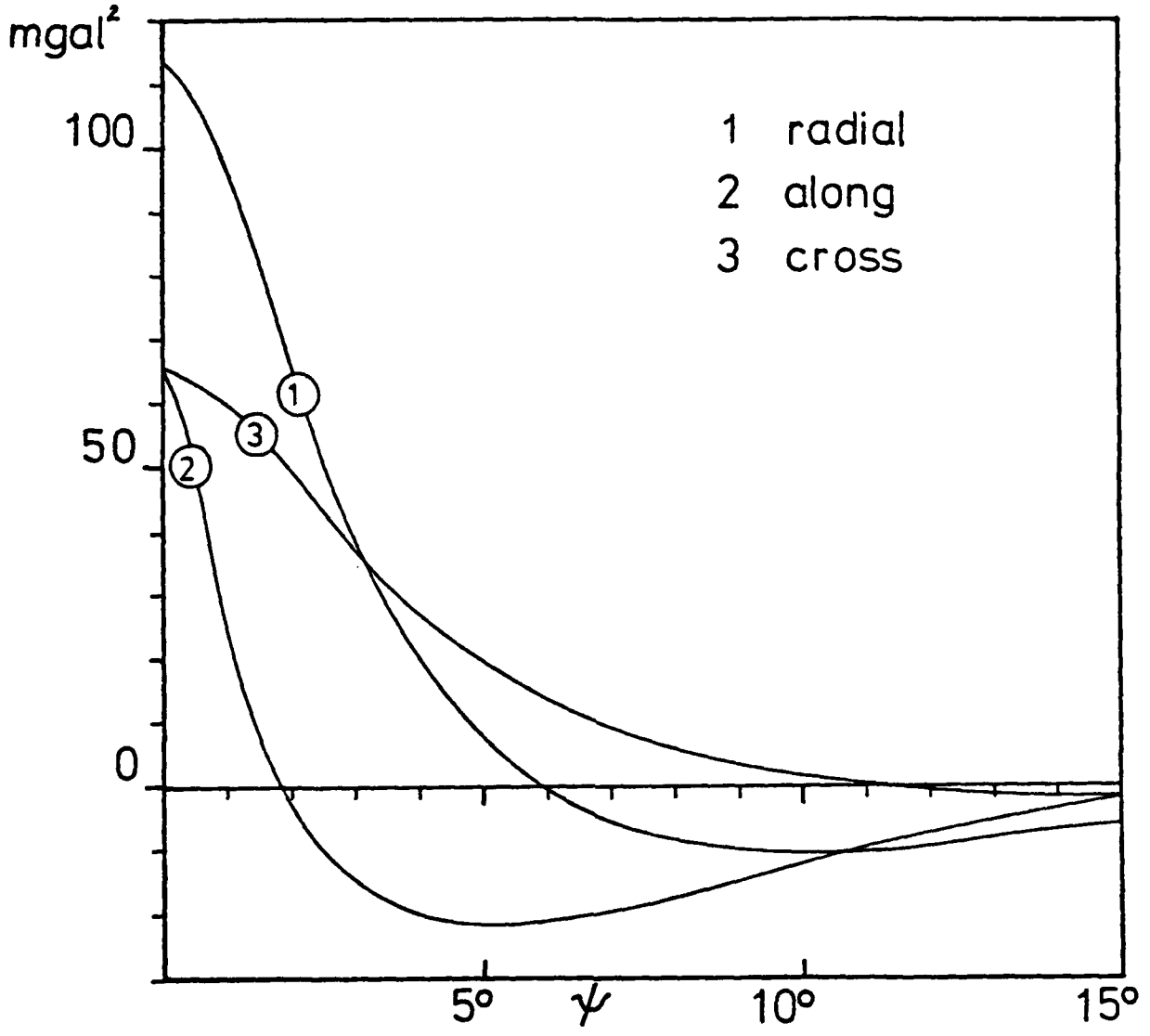

Figure 6a. Cross-covariance function between a surface gravity anomaly and acceleration differences at an altitude of 200 km and a seperation of 250 km (P with $\varphi = 0°$ and $\lambda = 0°$; P_a with $\varphi = \psi$ and $\lambda = 0°$)

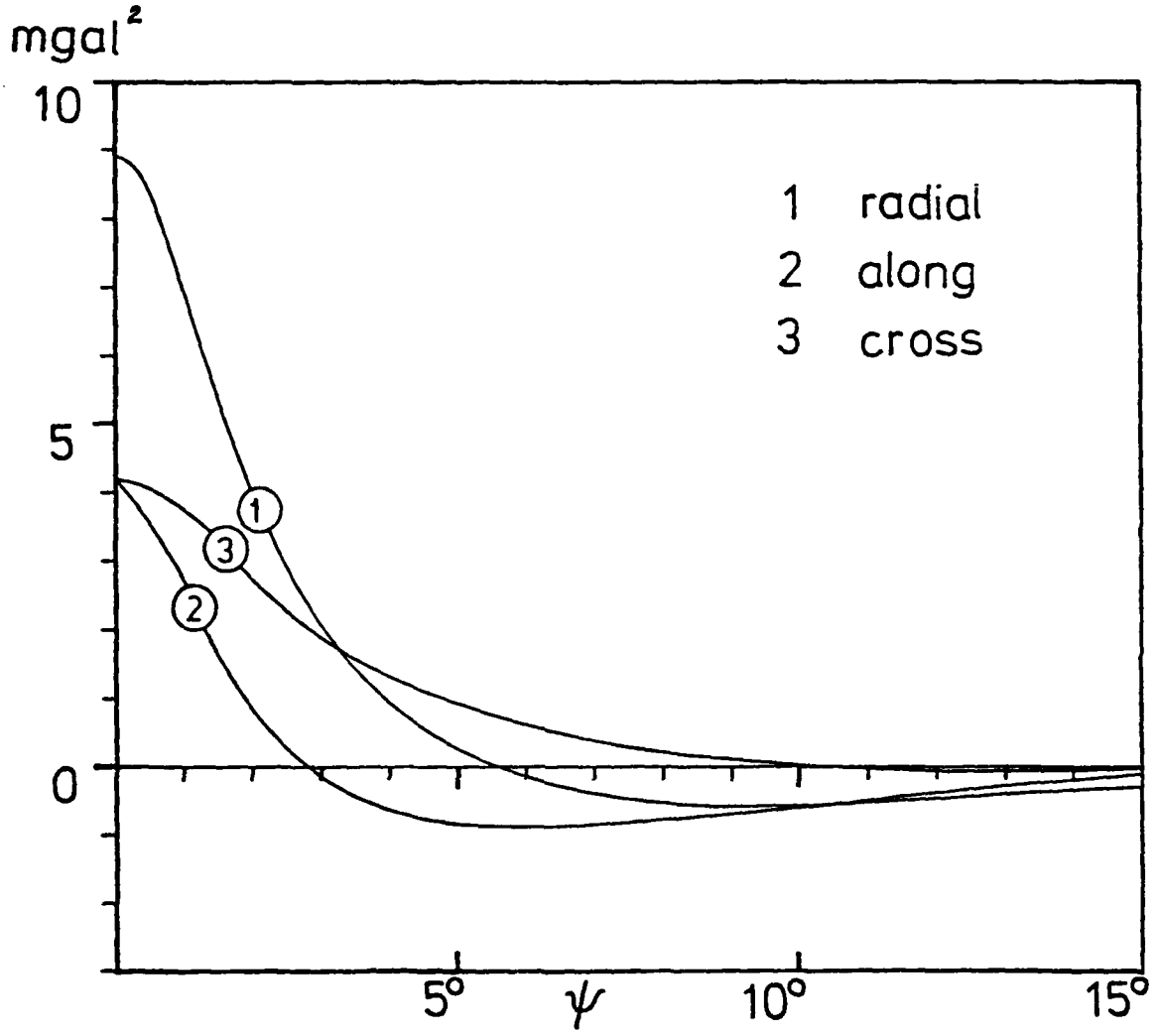

Figure 6b. Cross-covariance function between a surface gravity anomaly and acceleration differences at an altitude of 200 km and a separation of 10 km (P_1 with $\varphi = 0°$ and $\lambda = 0°$; P_2 with $\varphi = \psi$ and $\lambda = 0°$).

Next, the impact of the separation of the two satellites on the standard deviation of the estimated mean gravity anomaly has been investigated. Figure 7 contains the graphs for $\sigma(\overline{\Delta g})$ for a radial separation of 10 km, 50 km, and 250 km. In all cases the lower satellite is at an altitude of 200 km. The contribution of $\underline{L}\,\underline{D}\,\underline{L}^T$, equation (23), is given, too. As to be expected, the accuracy of the estimated gravity anomalies improves with increasing separation, if $\sigma(\ddot{\rho})$, or $\sigma(\dot{\rho})$ respectively, is kept constant. This result is discussed already in Rummel (1978) based on purely theoretical considerations.

Figure 7. Variation of the estimated a posteriori standard deviation of a 1° x 1° mean gravity anomaly with changing intersatellite distance (altitude: 200 km; radial separation) and the contribution of $\underline{L}\,\underline{D}\,\underline{L}^T$ (eqn. (23)).

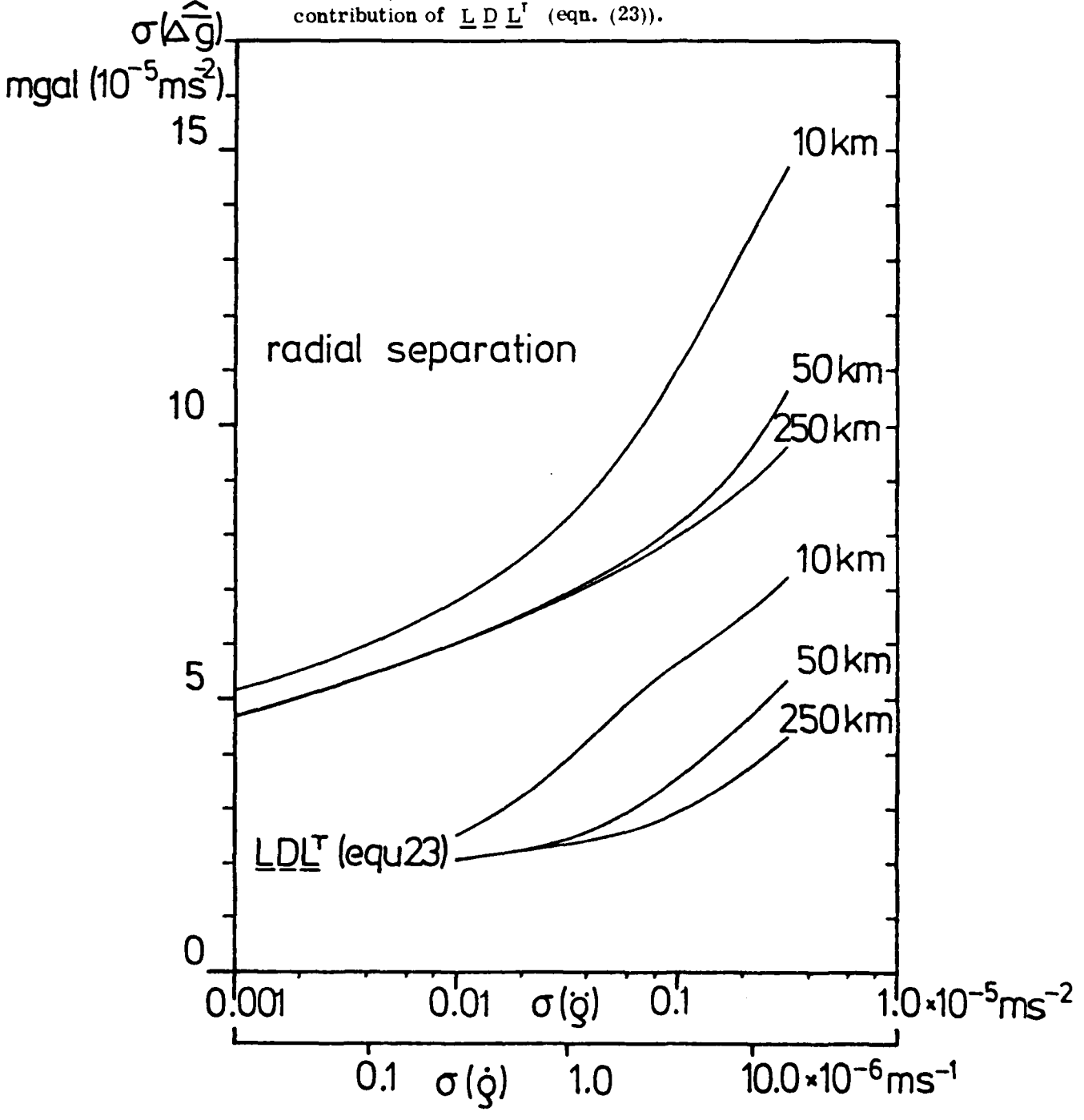

But not only the standard deviation of the estimates should be analyzed. Small correlations are a measure of a high mathematical independence of the estimated parameters. For block no. 2 (figure 2) and for an optimum of observational precision attainable in a gravitational satellite mission - ± 0.03 mgal for $\sigma(\ddot{\rho})$ or $\pm 10^{-6}$ ms^{-1} for $\sigma(\dot{\rho})$, respectively - the standard deviation of the a posteriori estimates and the correlations are presented in tables 2a through 2f. They contain on the main diagonal the standard deviation of all six considered $1^\circ \times 1^\circ$ blocks and on the off-diagonals the correlations among them. The results are given for radial, along track, and cross track separations of 10 km and 250 km at an altitude of 200 km. For radial separation almost perfect independence is achieved. The results for along track and cross track separation show a somewhat higher correlation in the direction of the separation. Again, this higher correlation would decrease with data covering a larger area.

Table 2a. Standard deviation and correlations for the six $1^\circ \times 1^\circ$ mean gravity anomalies.

1	2	3	4	5	6	
8.4	-0.23	0.11	-0.14	-0.10	0.06	1
	8.2	-0.23	-0.10	-0.17	-0.11	2
		8.3	0.06	0.11	0.14	3
			8.4	-0.28	0.13	4
				8.1	0.26	5
					8.2	6

radial
$\sigma(\ddot{\rho}) = \pm 0.03$ mgal
$(\triangleq \sigma(\dot{\rho}) = \pm 10^{-6}$ ms$^{-1})$
$r_1 = 200$ km
sep. 10 km

Table 2b. Standard deviation and correlations for the six $1^\circ \times 1^\circ$ mean gravity anomalies.

1	2	3	4	5	6	
12.7	-0.02	-0.03	0.35	0.02	0	1
	13.3	0.10	0.23	0.41	0.02	2
		13.5	0.08	0.27	0.40	3
			12.8	0.07	0.05	4
				13.1	0.11	5
					13.4	6

along track
$\sigma(\ddot{\rho}) = \pm 0.03$ mgal
$(\hat{=} \sigma(\dot{\rho}) = \pm\ 10^{-6}\ \mathrm{ms}^{-1})$
$r_1 = 200$ km
sep. 10 km

Table 2c. Standard deviation and correlations for the six $1^\circ \times 1^\circ$ mean gravity anomalies.

1	2	3	4	5	6	
15.1	0.55	0.52	0.21	0.25	0.34	1
	14.7	0.53	0.26	0.19	0.25	2
		14.8	0.34	0.25	0.27	3
			15.3	0.52	0.52	4
				14.6	0.53	5
					14.8	6

cross track
$\sigma(\ddot{\rho}) = \pm 0.03$ mgal
$(\hat{=} \sigma(\dot{\rho}) = \pm 10^{-6}\ \mathrm{ms}^{-1})$
$r_1 = 200$ km
sep. 10 km

Table 2d. Standard deviations and correlations for the six $1° \times 1°$ mean gravity anomalies.

1	2	3	4	5	6	
6.9	-0.10	0.09	-0.32	-0.10	-0.02	1
	6.8	-0.04	-0.10	-0.31	-0.10	2
		6.9	-0.02	-0.11	-0.32	3
			6.5	-0.07	0.09	4
				6.6	-0.04	5
					6.7	6

radial
$\sigma(\ddot{\rho}) = \pm 0.03$ mgal
$(\triangleq \sigma(\dot{\rho}) = \pm 10^{-6}\ ms^{-1})$
$r_1 = 200$ km
sep. 250 km

Table 2e. Standard deviations and correlations for the six $1° \times 1°$ mean gravity anomalies.

1	2	3	4	5	6	
9.3	0.12	0.34	0.04	0.15	0.26	1
	9.9	0.02	0.27	0.07	-0.01	2
		10.4	0.19	0.18	0.09	3
			10.4	0.11	0.13	4
				10,8	0.02	5
					11.3	6

along track
$\sigma(\ddot{\rho}) = \pm 0.03$ mgal
$(\triangleq \sigma(\dot{\delta}) = \pm\ 10^{-6}\ ms^{-1})$
$r_1 = 200$ km
sep. 250 km

Table 2f. Standard deviations and correlations for the six $1^\circ \times 1^\circ$ mean gravity anomalies.

1	2	3	4	5	6	
12.9	0.50	0.70	0.29	0.28	0.40	1
	13.0	0.48	0.29	0.30	0.28	2
		12.9	0.39	0.28	0.31	3
			13.4	0.53	0.67	4
				13.1	0.48	5
					12.8	6

cross track
$\sigma(\dot{p}) = \pm 0.03$ mgal
$(\hat{=} \sigma(\dot{p}) = \pm 10^{-6}\ ms^{-1})$
$r_1 = 200$ km
sep. 250 km

Another important factor influencing the quality of the estimated gravity parameters is the altitude at which the experiment is performed. Figure 8 gives the results analogous to figures 4 and 7 but now with a constant radial separation of 50 km and for altitudes of 150 km, 200 km, 250 km and 300 km. The attainable ±5 mgal for a $1^\circ \times 1^\circ$ mean gravity anomaly from only 74 observations of an altitude of 150 km would make it definitely worthwhile to fly the experiment at this low altitude if the related technical problems could be controlled. The increase of the accuracy with decreasing altitude is very distinct. Table 3 contains the results for all six blocks analogous to tables 2 for an altitude 150 km.

Figure 8. Variation of the estimated a posteriori standard deviation of a $1^\circ \times 1^\circ$ mean gravity anomaly with changing experiment altitude (radial separation of 50 km) and the contribution of $\underline{L}\,\underline{D}\,\underline{L}^T$ (eqn. (23)).

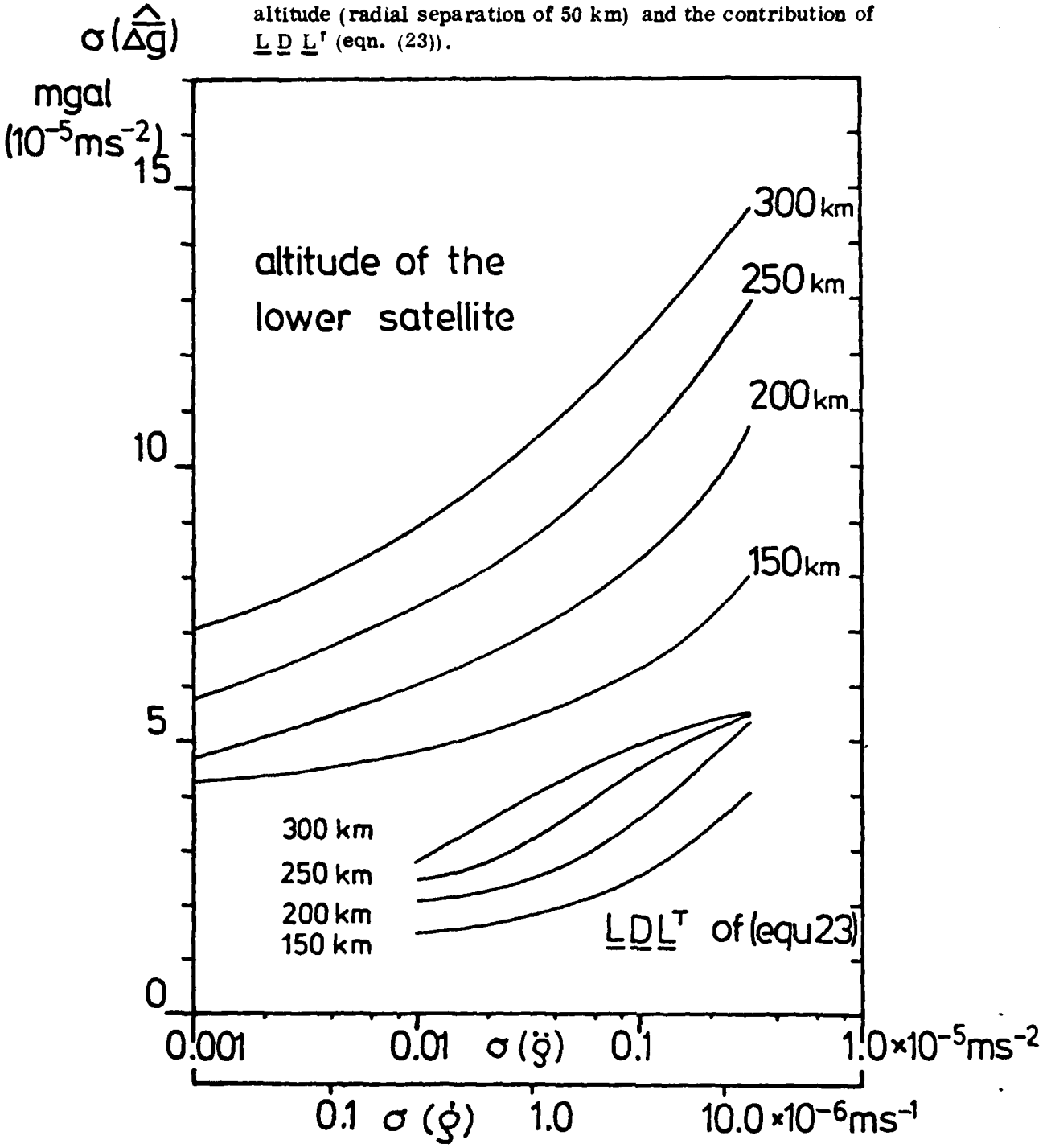

Table 3. Standard deviations and correlations for the six $1^\circ \times 1^\circ$ mean anomalies for an experiment altitude of 150 km and a radial separation of 50 km.

1	2	3	4	5	6	
5.1	0.06	-0.02	-0.31	-0.06	0.01	1
	5.4	0.12	-0.06	-0.29	-0.06	2
		5.4	0.01	-0,06	-0.30	3
			4.8	0.09	-0.01	4
				5.1	0.12	5
					5.1	6

radial
$\sigma(\ddot{\rho}) = \pm 0.03$ mgal
$(\triangleq \sigma(\rho) = \pm\ 10^{-6}\ ms^{-1})$
$r_1 = 150$ km
sep. 50 km

Finally, with a less optimal arrangement of the sample points with respect to the $1^\circ \times 1^\circ$ blocks - shown in figure 9 - the whole analysis has been repeated. Representative for these results are the numbers for the six blocks given in table 4 derived for a radial separation of 250 km at an altitude of 200 km. They show, when compared with table 2d, a significant decrease in the accuracies of approximately 20%.

Figure 9. Suboptimal arrangement of sample points (compare with figure 3).

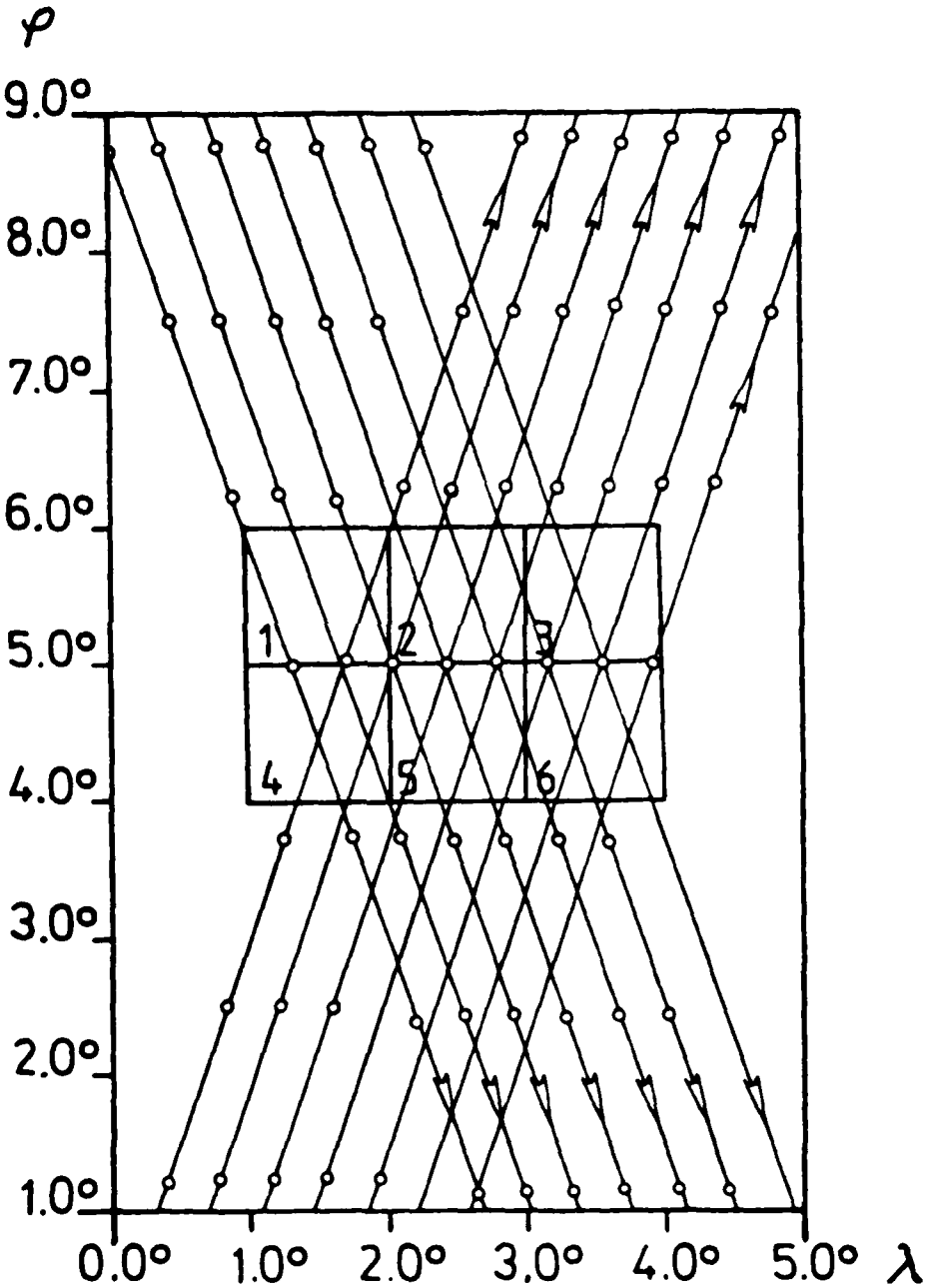

Table 4. Standard deviations and correlations for the six $1^\circ \times 1^\circ$ mean anomalies with a suboptimal arrangement of the sample points.

1	2	3	4	5	6	
8.4	0.0	0.06	-0.49	-0.20	0.03	1
	8.4	0.02	-0.24	-0.62	-0.23	2
		8.6	0.03	-0.21	-0.56	3
			9.1	-0.07	0.08	4
				8.5	0.02	5
					8.8	6

radial
$\sigma(\ddot{\rho}) = \pm$ 0.03 mgal
$(\hat{=} \sigma(\dot{\rho}) = \pm 10^{-6}\ \mathrm{ms}^{-1})$
$r_1 = 200$ km
sep. 250 km

Geoid Heights and Geoid Height Differences

In figure 10 the ground tracks are shown together with the locations for which the a posteriori variances of geoid heights and geoid height differences have been estimated (x). Also contained are so called suboptimal locations (Δ).

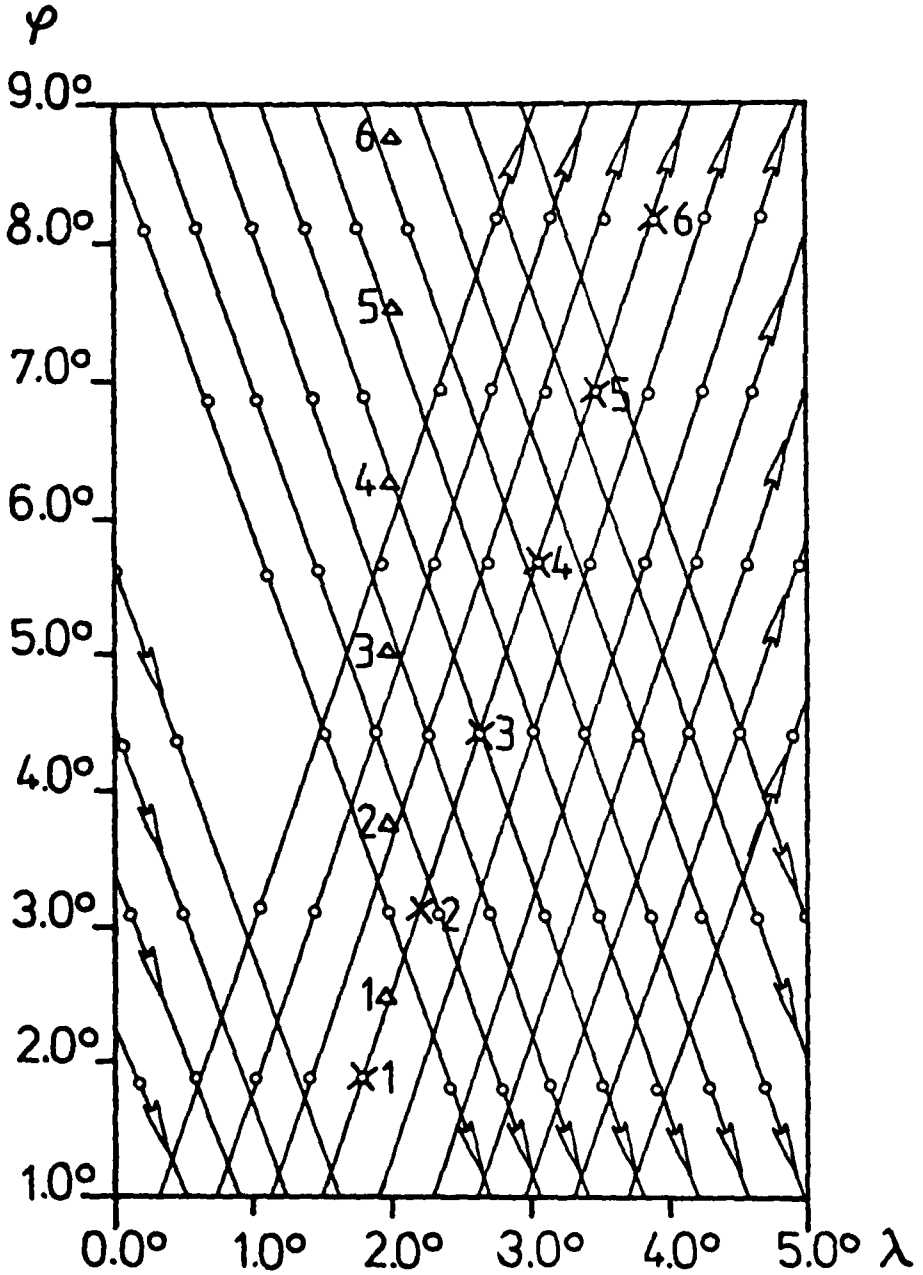

Figure 10. Groundtracks with the locations of the points for which geoid heights are estimated ("x" optimal locations; "Δ" arbitrary arrangement).

The estimation of geoid height differences is discussed in Christodoulidis (1976) and Jekeli (1979). The a posteriori variance of a geoid height difference δN between two points P_1 and P_2 is derived from the variances and covariances of the point estimates by:

$$\sigma^2\{\delta N(P_2 - P_1)\} = \sigma^2\{N(P_2)\} - 2\,\mathrm{cov}\{N(P_2); N(P_1)\} + \sigma^2\{N(P_1)\} \quad (30)$$

Equation (30) indicates that mainly high correlations are responsible for low variances or standard deviations of the geoid height differences. To me it seems therefore no principal advantage to estimate differences of a quantity instead of the quantity itself, except for the aspect of eliminating systematic errors with long wavelength structure. Quite in contrast, equation (30) shows that for independent estimates the standard deviation of a difference is $\sqrt{2}$ times that of the point estimate. The characteristic of estimating differences is to be distinguished from measuring differences, as e.g. in gravimetry, where the advantage may come from the measurement principle.

The results will be given for point no. 3 and for geoid height differences between points no. 3 and 4 (151 km) and points no. 3 and 5 (302 km). Figure 11 shows the a posteriori standard deviation of the estimated geoid height $N(P_3)$ and geoid height differences $\delta N(P_4 - P_3)$ and $\delta N(P_5 - P_3)$ as a function of the observational precision σ ($\dot{\rho}$). The experiment altitude is 200 km and the separation 250 km in radial, along track and cross track direction.

Again, observational data covering a larger area would produce estimates of similar quality for along and cross track separation as for radial separation. The optimal number of approximately ± 0.70 m is achieved for $\delta N(3\text{-}4)$ in radial separation. As to be expected from equation (30) the results for geoid height differences depend very much on the correlation between the point estimates. This produces usually a pattern of increasing a posteriori standard deviations for geoid height differences with increasing distance of the two points, and point estimates slightly worse than the geoid height differences for small distances. Especially good estimates for geoid height differences are obtained when the two points are located along the direction of separation of the two satellites, either along or cross track.

The dependence on the separation distance of the two satellites is displayed in figure 12. In all cases a radial separation of an altitude of 200 km is assumed. As for mean gravity anomaly estimates the results improve with increasing inter-satellite distance.

Figure 11. Estimated a *posteriori* standard deviation of the geoid height $N(P_3)$ and the geoid height differences $\delta N(P_4-P_3)$, (150 km), and $3\,\delta N(P_5-P_3)$, (300 km), as a function of the a priori range rate change or range rate precision in dependence of the spatial arrangement of the two satellites (a...along track, c...cross track, r...radial; altitude 200 km; separation 250 km).

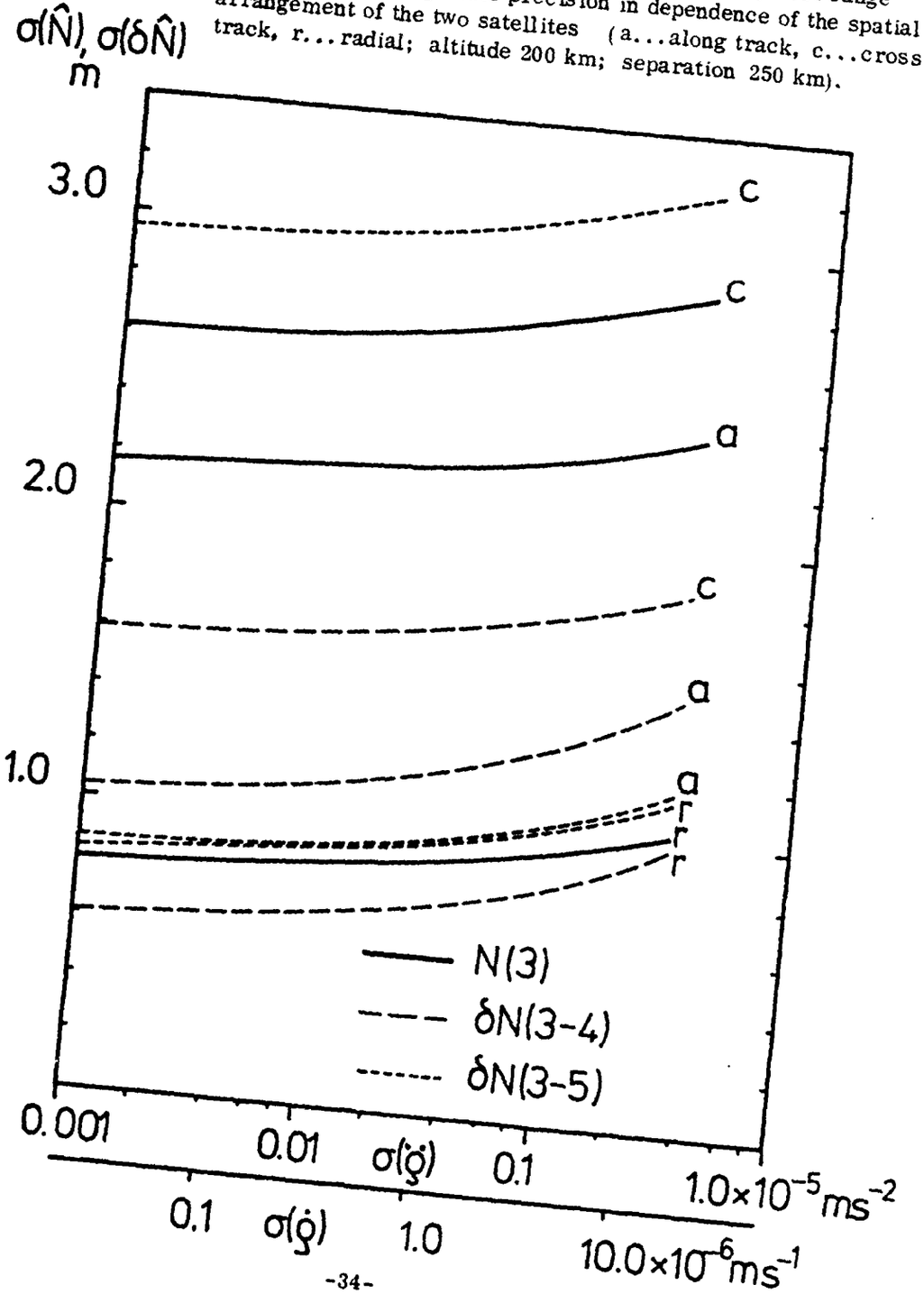

Figure 12. Variation of the estimated a posteriori standard deviation of the geoid height $N(P_3)$ and the geoid height differences $\delta N(P - P_3)$ and $\delta N(P_5 - P_3)$ with changing separation of the two satellites (altitude: 200 km; radial separation).

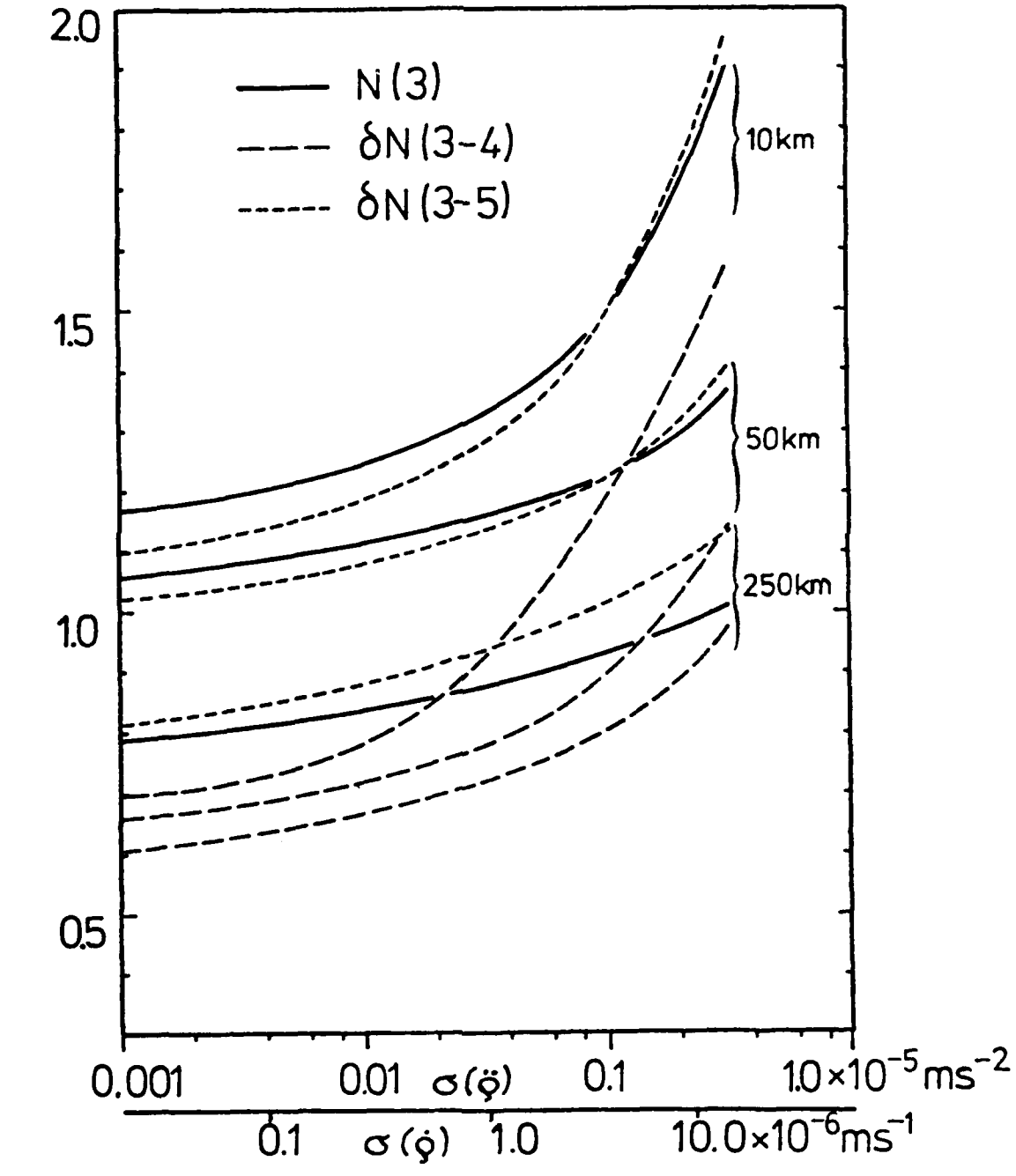

Rather heterogeneous looks the picture for the analysis of the dependence of the estimates on the experiment altitude, shown in figure 13. The standard deviation of the point estimates increase with decreasing experiment altitude. The reason for this paradox result is again the comparably small area covered by the sampling points. For, the cross-covariance function between surface geoid heights and the radial component of the disturbing potential shows a first zero at about 7° with a comparably high correlation for large spherical distances. For geoid height differences the a posteriori standard deviation would agree with the anticipated behavior - decreasing standard deviation with decreasing experiment altitude - but only for very low range rate change or range rate noise level.

Finally, the results for points located along a ground track (" x " in figure 10) are compared with those for points located arbitrarily, somewhere between the ground tracks (" Δ " in figure 10). Table 5 contains the a posteriori standard deviation for three point geoid height estimates and two standard deviations for geoid height differences, all for a radial, along and cross track separation of 250 km at 200 km altitude, and for a radial separation of 50 km at 150 km and 200 km. The left of each pair of columns shows the numbers for the optimal point locations, the right columns those for the arbitrary locations. A significant dependence on the point location can only be seen for radial separations whereas for along and cross track separations the point location plays no distinct role.

Table 5. Estimated standard deviation for geoid heights and geoid height differences assuming a range rate change precision of ±0.03 mgal for an optimal and an arbitrary location of the estimation points, see figure 10 (altitude/separation).

$\sigma(\ddot{\rho}) = 0.03$ mgal ($\sigma(\dot{\rho}) = 10^{-6}$ m s^{-1})	radial 200/250		along track 200/250		cross track 200/250		radial 150/50		radial 200/50	
	opt.	arb.	opt.	arb.	opt.	arb.	opt.	arb.	opt.	arb.
	m	m	m	m	m	m	m	m	m	m
$N(P_3)$	0.89	0.94	2.22	2.23	3.03	3.04	1.36	1.42	1.17	1.20
$N(P_4)$	0.90	1.01	2.24	2.28	3.01	3.02	1.40	1.53	1.18	1.31
$N(P_5)$	1.08	1.15	2.31	2.47	3.03	3.06	1.65	1.78	1.41	1.49
$\delta N(P_4 - P_3)$	0.72	0.98	0.94	0.95	1.67	1.76	0.73	1.03	0.77	1.04
$\delta N(P_5 - P_3)$	0.94	0.96	1.17	1.41	2.69	2.69	1.23	1.29	1.13	1.14

Figure 13. Variation of the estimated a posteriori standard deviation of the geoid height $N(P_3)$ and the geoid height differences $\delta N(P_4 - P_3)$ and $\delta N(P_5 - P_3)$ with changing experiment altitude, given in km (radial separation of 50 km).

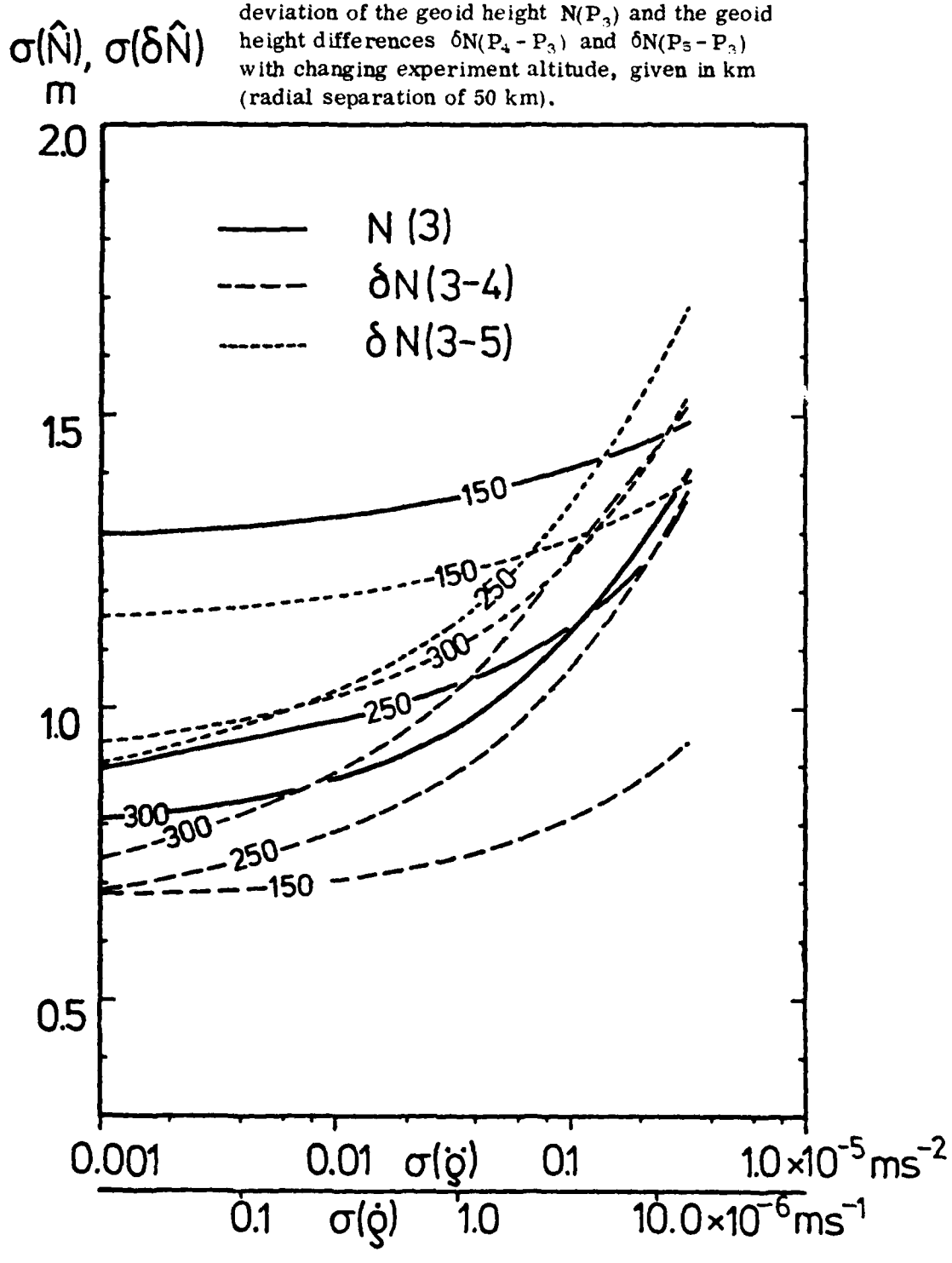

Information Content Per Frequency

Of special importance for the user is that the estimated gravity parameters really contain information down to a half wavelength of 100 km, or up to $\ell \doteq 180$ in terms of spherical harmonics. We computed therefore from the given data the variance and standard deviation of the geoid height of point no. 3 for the frequency ranges $\{\ell \mid 13 \leq \ell < \infty\}$, $\{\ell \mid 121 \leq \ell < \infty\}$, and $\{\ell \mid 181 \leq \ell < \infty\}$ separately and compared the information contained in the ranges 13-120, 121-180, 181-∞. Table 6a gives the values for the a priori standard deviation, a posteriori standard deviation and the ratio of a posteriori to a priori variance for the three spectral ranges for a radial separation of 250 km and an altitude of 200 km. Table 6b contains the corresponding information for a radial separation of 10 km.

The ratios of the a posteriori to a priori variance indicate that

- considerable information is contained in the frequency range from 121 to 180 (1:15),
- almost no information has been extracted from frequencies higher than $\ell = 180$ (1:1.2 and 1:1.7 respectively)
- the improvement of the larger separation of 250 km against that of only 10 km comes only from the low frequencies (1:52 versus 1:22).

Table 6a. A priori and a posteriori standard deviation and ratio of the a priori to the a posteriori variances for three spectral ranges (altitude: 200 km; radial separation 250 km).

	spectral ranges		
	13 - 120	121 - 180	181 - ∞
a priori r.m.s.	5.47	0.53	0.46
a posteriori r.m.s.	0.76	0.14	0.36
$\frac{\text{a post. var.}}{\text{a priori var.}}$	1:52	1:15	1:1.7

Table 6b. A priori and a posterori standard deviation and ratio of the a posteriori to the a priori variances for three spectral ranges (altitude: 200 km; radial separation 10 km).

	spectral ranges		
	13 - 120	121 - 180	181 - ∞
a priori r.m.s.	5.47	0.53	0.46
a posteriori r.m.s.	1.17	0.14	0.42
$\frac{\text{a post. var.}}{\text{a priori var.}}$	1:22	1:15	1:12

6. Summary and Conclusions

The goal of this study was an error analysis for $1^\circ \times 1^\circ$ mean gravity anomalies, point geoid heights, and geoid height differences derived from observations in a "low-low" satellite-to-satellite tracking experiment. The chosen estimation method was least squares collocation. In order to facilitate the mathematical model not the range rates themselves but their time derivatives, i.e. range rate changes or line of sight accelerations, were assumed to be given.

The orbit requirements were treated separately in an empirical sensitivity study. If we assume a range rate change precision of ± 0.03 mgal ($\hat{=} 10^{-6}$ m s^{-1}) and want to keep systematic errors below 1/10 of this level, unmodelled high frequency disturbances, in the orbit, e.g. due to drag effects, would have to be kept below 1 cm in radial direction, and 1.5 m in along or cross track direction. Thus, a drag-free capability or a system of micro-accelerometers seems to be necessary. Unmodelled long wavelength errors modulated by short wavelength model coefficients have to be kept smaller than around 10 m independent of the direction of the separation, and should therefore be no limiting factor.

The a posteriori standard deviations of the $1^\circ \times 1^\circ$ mean gravity anomalies were analyzed as a function of the experiment altitude, the separation, the spatial arrangement of the two satellites, and the location of blocks with respect to the sample points. For a separation of 250 km of 200 km altitude and a range rate precision of ± 0.03 mgal a standard deviation of ± 6.5 mgal was derived, with almost no correlation between the individual blocks.

The same criteria, i.e. experiment altitude, separation, spatial arrangement of the satellites, and the location of the points with respect to the sample points, were examined for geoid heights and geoid height differences. The results for geoid height differences depend mainly on the level of correlation between the point estimates. For small distances, e.g. 150 km, they become as low as 0.65 m (altitude 200 km, separation 250 km, $\sigma(\ddot{\rho}) = \pm 0.03$ mgal). For point geoid heights (and the same situation as above) about ± 0.80 m are feasible. In addition, the information content in the three frequency ranges from degree 13 to 120, 121 to 180, and 181 to infinity was investigated separately. The decrease of the a priori variance by a factor of 12 in the frequency range from 121 to 180 shows that sufficient short-wavelength information - down to half wavelengths of 100 km - can be deduced from the low-low SST experiment. Throughout the analysis a reference field up to degree 12 was assumed to be known perfectly.

Whereas the results for mean gravity anomalies would satisfy in resolution as well as in accuracy the defined demands of geophysicists, the obtained numbers for geoid heights and geoid height differences are not sufficient for most oceanographic purposes. On the other hand, it is worthwhile to remember that the derived geoid height precision of ± 0.80 m is very well comparable with the excellent result for sea surface topography, as obtained from GEOS-3 altimetry.

References

Applications of a Dedicated Gravitational Satellite Mission, National Academy of Sciences, Washington, D.C., 1979.

Barthel, G., T. Halldorsson, H. Hufnagel, D. Meissner, Ch. Schmidt, Laser Ranging Instrumentation, Final Report, Messerschmitt-Bölkow-Blohm, Space Division RX 12, München, 1978.

Christodoulidis, D. C., On the Realization of a 10 cm Relative Ocean Geoid, Department of Geodetic Science, Report No. 247, The Ohio State University, Columbus, 1976.

Douglas, B. C., C. C. Goad, F. F. Morrison, Determination of the Geopotential from Satellite-to-Satellite Tracking Data, NOAA Techn. Memo. NOS NGS 24, Rockville, 1980.

Eddy, W., R. Sutermeister, Satellite-to-Satellite Measurements, Wolf Research and Development Group, Riverdale, Maryland, 1975.

Grafarend, E., The Bruns Transformation and a Dual Setup of Geodetic Observational Equations, preprint NOAA NOS NGS Report, Rockville, 1979.

Hajela, D. P., Improved Procedures for the Recovery of 5° Mean Gravity Anomalies from ATS-6/GEOS-3 Satellite-to-Satellite Range-Rate Observations, Department of Geodetic Science, Report No. 276, The Ohio State University, Columbus, 1978.

Heiskanen, W. A., H. Moritz, Physical Geodesy, Freemann and Co., San Francisco, 1967.

Jekeli, Ch., Global Accuracy Estimates of Point and Mean Undulation Differences Obtained from Gravity Disturbances, Gravity Anomalies and Potential Coefficients, Department of Geodetic Science, Report No. 288, The Ohio State University, Columbus, 1979.

Kaula, W. M., G. Cherubini, N. Burkhard, D. D. Jackson, Applications of Inversion Theory to New Satellite Systems for Determination of the Gravity Field, Final Report, Department of Earth & Space Sciences, University of California, Los Angeles, 1978.

Krynski, J., Possibilities of Low-Low Satellite Tracking for Local Geoid Improvement, Mitteilungen der geodätischen Institute der TU 37, Graz, 1978.

Moritz, H., Advanced Least-Squares Methods, Department of Geodetic Science, Report No. 175, The Ohio State University, Columbus, 1972.

Muller, P. M., W. L. Sjogren, Mascons: Lunar Mass Concentrations, Science, 161, pp. 680-684, 1968.

Rapp, R. H., D. P. Hajela, Accuracy Estimates of $1^{\circ} \times 1^{\circ}$ Mean Anomaly Determinations from a High-Low SST Mission, Department of Geodetic Science, Report No. 295, The Ohio State University, Columbus, 1979.

Reed, G. B., Application of Kinematical Geodesy for Determining the Short Wave Length Components of the Gravity Field by Satellite Gradiometry, Department of Geodetic Science, Report No. 201, The Ohio State University, Columbus, 1973.

Rummel, R., Determination of Short-Wavelength Components of the Gravity Field from Satellite-to-Satellite Tracking or Satellite Gradiometry - An Attempt to an Identification of Problem Areas, manuscripta geodaetica, 4, pp. 107-148, 1979.

Rummel, R., D. P. Hajela, R. H. Rapp, Recovery of Mean Gravity Anomalies from Satellite-to-Satellite Range Rate Data Using Least Squares Collocation, Department of Geodetic Science, Report No. 248, The Ohio State University, Columbus, 1976.

Rummel, R., Ch. Reigber, K. H. Ilk, The Use of Satellite-to-Satellite Tracking for Gravity Parameter Recovery, Proc. European Workshop Space Oceanography, Navigation and Geodynamics, ESA SP 137, pp. 153-161, 1978.

Rummel, R., K.-P. Schwarz, M. Gerstl, Least Squares Collocation and Regularization, Bull. Geod., 53, pp. 343-361, 1979.

Schwarz, C., Gravity Field Refinement by Satellite-to-Satellite Doppler Tracking, Department of Geodetic Science, Report No. 147, The Ohio State University, Columbus, 1970.

Sünkel, H., A Covariance Approximation Procedure, Department of Geodetic Science, Report No. 286, The Ohio State University, Columbus, 1979.

Tscherning, C. C., Covariance Expressions for Second and Lower Order Derivatives of the Anomalous Potential, Department of Geodetic Science, Report No. 225, The Ohio State University, Columbus, 1976.

Tscherning, C. C., R. H. Rapp, Closed Covariance Expressions for Gravity Anomalies, Geoid Undulations and Deflections of the Vertical Implied by Anomaly Degree Variance Models, Department of Geodetic Science, Report No. 208, The Ohio State University, Columbus, 1974.

Wolff, M., Direct Measurements of the Earth's Gravitational Potential Using a Satellite Pair, Journal Geophys. Res., 14, pp. 5295-5300, 1969.

Appendix

The degree variance model underlying all further derivations is the one published by Tscherning and Rapp (1974) for gravity anomalies

$$\sigma_\ell^2(\Delta g) = s^{\ell+2} \frac{A\,(\ell-1)}{(\ell-2)(\ell+B)} = s^{\ell+2}\, c_\ell\,, \tag{A1}$$

where $s = (r_{Bje}^2 / r_P^2)$ is the square ratio of the radius of an adopted Bjerhammar sphere and the geocentric distance of the point under consideration, $A = 425.28$ mgal^2 and $B = 24$. Then the degree variances of the disturbing potential, and of the radial and horizontal components of the gradient of the disturbing potential become:

$$\sigma_\ell^2(T) = s^{\ell+1} \frac{r_{Bje}^2}{(\ell-1)^2}\, c_\ell\,, \tag{A2}$$

$$\sigma_\ell^2(\delta_r) = s^{\ell+2} \left(\frac{\ell+1}{\ell-1}\right)^2 c_\ell\,, \text{ and} \tag{A3}$$

$$\sigma_\ell^2(\delta_\varphi) = \sigma^2(\delta_\lambda) = \tfrac{1}{2}\, s^{\ell+2}\, \frac{\ell\,(\ell+1)}{(\ell-1)^2}\, c_\ell\,. \tag{A4}$$

The square of the velocity difference of two satellites is, according to e.g. Wolff (1969), approximated by $\underline{\delta\dot{X}}_{12}^2 \doteq \frac{1}{\dot{\underline{X}}^{c2}}\, T_{12}^2$ where $\dot{\underline{X}}^{c2} = \left(\frac{GM}{r_P}\right)$ is the mean velocity. Thus the degree variance model for a velocity difference for instance in radial direction becomes:

$$\sigma_\ell^2(|\underline{\delta\dot{X}}_{12}|) = \frac{1}{\dot{\underline{X}}^{c2}} \left(1 - \left(\frac{r_P}{r_Q}\right)^{\ell+1}\right)^2 \sigma_\ell^2(T) \tag{A5}$$

with r_P and r_Q the geocentric radii of the two satellites. Similarily, the degree variance model for an acceleration difference, again in radial direction, is:

$$\sigma_\ell^2(\ddot{\underline{X}}_{12}^r) = \left(1 - \left(\frac{r_Q}{r_P}\right)^{\ell+2}\right)^2 \sigma^2(\delta_r)\,. \tag{A6}$$

Equations (A5) and (A6) are slightly optimistic degree variance models for range rate, and range rate change signals. They are optimistic in the sense that one assumes the two satellites to be arranged in such a way that they either sense perfectly the radial or the horizontal component. Finally, the degree variance model for the second radial derivative is

$$\sigma_\ell^2(T^{rr}) = s^{\ell+3}\, \frac{(\ell+1)^2\,(\ell+2)^2}{r_{Bje}^2\,(\ell-1)^4}\, c_\ell\,. \tag{A7}$$

A comparison of signal and noise requires a degree or degree-order model for the noise, too. We postulate white noise behavior and approximate its covariance function by a first-order Gauss-Markov model, e.g. for range rates:

$$\epsilon^2(\dot{\rho}) = m_o^2 \, e^{-c\psi} \tag{A8}$$

with m_o^2 ... variance of the random observation error,
c ... inverse correlation length, and
ψ ... spherical distance.

A harmonic analysis on the sphere yields for a coefficient of degree l and order m of the noise process:

$$\epsilon^2_{lm}(\dot{\rho}) = \frac{1}{2} \frac{m_o^2}{c^2} \tag{A9}$$

The inverse correlation length c (units of arc) is derived from the correlation length in time units, t_c, or length units, s_c, by:

$$c^2 = \frac{p}{2\pi t_c} = \frac{r_p}{s_c} \tag{A10}$$

where $p = 2\pi (r_p^3/GM)^{\frac{1}{2}}$ is the orbital period. Equation (A9) holds for the degree-order variance of the noise of any type of observed quantity if only the corresponding noise variance and correlation length are inserted.